

# Kinematically Extended Continuum Theories: Correlation Between Microscopical Deformation and Macroscopical Strain Measures

T. Ebinger, H. Steeb, S. Diebels

*The present work investigates the correlation between macroscopical deformation modes and microscopical deformation modes. Thereby, the macroscopical deformation is represented by the strain-like quantities of the according macroscopical continuum theory while the microscopical deformation is expressed in the form of a Taylor series expansion. The use of an energy criterion makes it possible to derive a quantitative relation between microscopical and macroscopical deformation. The procedure is applied to different kinematically extended continuum theories on the macroscopical level. The investigation may help to select an optimal macroscopical continuum theory instead of choosing a theory based on phenomenological observations, whereby the optimal theory is that one, which reflects the microscopical deformation behaviour best. The microscopical deformation behaviour depends on the topology of the microstructure under consideration. Thus, the optimal theory is affected by the topology of the microstructure.*

## 1 Motivation

The deformation behaviour of a material body of dimension  $L$  with inherent microstructure of dimension  $l$  can be described either on a microscopical scale resolving the geometry of the microstructure with inherent microscopical material parameters or on a macroscopical scale by an appropriate continuum theory. While the macroscopic continuum theory assumes – as the name implies – that the material body is continuous, the theory may be extended accounting for the discontinuity of the material body. The microscopical deformation can be expressed in the form of a Taylor series expansion for the displacement field  $\mathbf{u}^m(\mathbf{x}, t)$ <sup>1</sup>, cf. Forest and Sab (1998); Forest (1999); Forest et al. (2000).

From a macroscopical point of view, the volume under study should be relatively large to be representative in a statistical sense. By contrast from a microscopical point of view, which motivates the Taylor series expansion, the volume should be relatively small, so that the expansion can be truncated after terms of a certain order while the contribution of the higher order terms can be neglected. Considering both aspects, the smallest material body is investigated, which is able to reflect the basic deformation behaviour. Accepting that this material body may not be representative in a statistical sense, according to Huet (1997) we call it Testing Volume Element (TVE). The TVE is required to reflect the fundamental deformation behaviour of the microstructure, but it does not necessarily have to be representative allowing for smaller volume elements compared to a Representative Volume Element (RVE) as discussed by, e. g., Nemat-Nasser and Hori (1993).

Depending on the continuum model describing the deformation behaviour on the macroscopical level, several terms of the Taylor series expansion correspond to strain-like quantities on the macroscopical level while other terms are not reflected by the continuum theory. E. g., in the case of the standard Boltzmann continuum theory only the linear terms of the expansion are considered on the macroscopical level while all terms of higher order are neglected. Regarding that the selection of a macroscopic continuum theory reduces the number of permitted deformation modes, the question arises, which may be the best macroscopic continuum theory for a certain microstructure with known topology. Usually the macroscopic continuum theory is chosen based on phenomenological observations like, e. g., size effects. Sometimes the choice is motivated by the underlying local deformation behaviour of the microstructure as, e. g., in the case of granular media, where the Cosserat continuum theory Cosserat and Cosserat (1909) is chosen according to the extra rotation of the single grains. However, quite often the macroscopical continuum theory is chosen based on phenomenological observations as in the case of foam-like microstructures, where the Cosserat theory is used to reflect the size effects observed in material testing. If the

<sup>1</sup>microscopic quantities are marked by superscript  $(\bullet)^m$ , macroscopic quantities by superscript  $(\bullet)^M$ .

macroscopical continuum theory is chosen without consideration of the microscopical deformation behaviour, it may occur that the macroscopical continuum theory is able to reflect deformation modes which are not observed on the microscopical level, while modes seeming to be important on that level are not considered on the macroscopical level. Obviously this will lead into difficulties for identifying the material parameters of such a material with inherent length scale, because a certain stiffness has to be assigned to a certain deformation mode not really being sensitive.

The present work demonstrates that the selection of the extended continuum theory is affected by the microscopic deformation behaviour of the TVE. Thereby, we restrict ourselves to kinematically extended continuum theories, which means gradient-based continuum theories, namely the second gradient theory (Germain (1973)) and the micromorphic continuum theory including the restricted cases, i. e., the Cosserat (Cosserat and Cosserat (1909)) or micropolar continuum theory and the microstretch theory. For an overview of kinematically extended continuum theories see Eringen (1999), Capriz (1980) and references cited therein. In the following we use the abbreviation "MMM theories" introduced by Eringen (1999) for the micromorphic, microstretch and micropolar continuum theories. However, in contrast to Eringen's definition of the microstretch theory, which allows only for an extra volumetric deformation (scalar quantity), we refer to the microstretch theory as the theory, which is able to reflect an extra directional stretch deformation (vector valued quantity).

## 2 Microscopical Deformation

Starting point of the considerations on the microscopical level is the assumption that the local displacement field  $\mathbf{u}^m(\mathbf{x}, t)$  of a certain domain, which can be identified with the Testing Volume Element (TVE), is expressed in the form of a Taylor series expansion

$$\begin{aligned} \mathbf{u}^m(\mathbf{x}, t) = & (\alpha_1 + \alpha_2 x + \alpha_3 y + \alpha_4 z + \alpha_5 x^2 + \alpha_6 y^2 + \alpha_7 z^2 + \alpha_8 xy + \alpha_9 xz + \alpha_{10} yz + \\ & \alpha_{11} x^3 + \alpha_{12} y^3 + \alpha_{13} z^3 + \alpha_{14} x^2 y + \alpha_{15} y^2 z + \alpha_{16} z^2 x + \alpha_{17} x y^2 + \alpha_{18} y z^2 + \\ & \alpha_{19} z x^2 + \alpha_{20} x y z + \alpha_{21} x^4 + \alpha_{22} y^4 + \alpha_{23} z^4 + \alpha_{24} x^2 y^2 + \alpha_{25} y^2 z^2 + \alpha_{26} z^2 x^2 + \dots) \mathbf{e}_x + \\ & (\beta_1 + \beta_2 x + \beta_3 y + \beta_4 z + \beta_5 x^2 + \beta_6 y^2 + \beta_7 z^2 + \beta_8 xy + \beta_9 xz + \beta_{10} yz + \\ & \beta_{11} x^3 + \beta_{12} y^3 + \beta_{13} z^3 + \beta_{14} x^2 y + \beta_{15} y^2 z + \beta_{16} z^2 x + \beta_{17} x y^2 + \beta_{18} y z^2 + \\ & \beta_{19} z x^2 + \beta_{20} x y z + \beta_{21} x^4 + \beta_{22} y^4 + \beta_{23} z^4 + \beta_{24} x^2 y^2 + \beta_{25} y^2 z^2 + \beta_{26} z^2 x^2 + \dots) \mathbf{e}_y + \\ & (\gamma_1 + \gamma_2 x + \gamma_3 y + \gamma_4 z + \gamma_5 x^2 + \gamma_6 y^2 + \gamma_7 z^2 + \gamma_8 xy + \gamma_9 xz + \gamma_{10} yz + \\ & \gamma_{11} x^3 + \gamma_{12} y^3 + \gamma_{13} z^3 + \gamma_{14} x^2 y + \gamma_{15} y^2 z + \gamma_{16} z^2 x + \gamma_{17} x y^2 + \gamma_{18} y z^2 + \\ & \gamma_{19} z x^2 + \gamma_{20} x y z + \gamma_{21} x^4 + \gamma_{22} y^4 + \gamma_{23} z^4 + \gamma_{24} x^2 y^2 + \gamma_{25} y^2 z^2 + \gamma_{26} z^2 x^2 + \dots) \mathbf{e}_z. \end{aligned} \quad (1)$$

Ensuring that the terms of lowest order, the constant terms, represent the barycentric displacement of the center of gravity  $S$ , so that in the case of neglecting all higher order terms at least the displacement of this characteristic point is reflected correctly, the coordinate system is attached just to that point, see Figure 1.

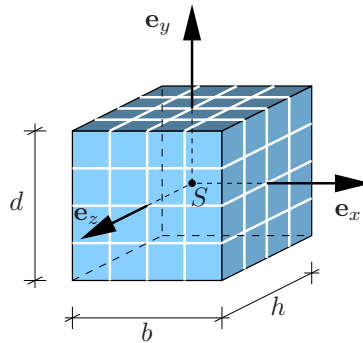


Figure 1: Cuboid TVE (dimensions  $b$ ,  $d$  and  $h$ ) and coordinate system

For the further investigations it is assumed that the topology and material parameters are known for the TVE. Thus, the deformed configuration can be calculated according to several terms of the Taylor series expansion (eq. (1)). However, physically it is not reasonable to allow for the application of Dirichlet boundary conditions in

the interior of the TVE. So the displacement field is only prescribed on the boundary of the TVE, which yields from a mathematical point of view a well-posed system of equations. From a physical point of view this yields the advantage that only observable quantities are used. The difference between the application of the displacement field to the boundary only, and application of the displacement field exactly in every point of the TVE may be clarified even for a homogeneous TVE of Boltzmann type<sup>2</sup>: while in the first case the ratio between tensile stiffness and shear stiffness has a strong influence on the deformed configuration for terms of quadratic order and higher (modes demonstrating a combined stretch and shear deformation on a microscopical level), in the second case the deformed configuration is completely prescribed and therefore independent of the topology and also independent of material parameters.

The according deformation modes for terms in  $e_x$ -direction are visualised up to order three in Figure 2.

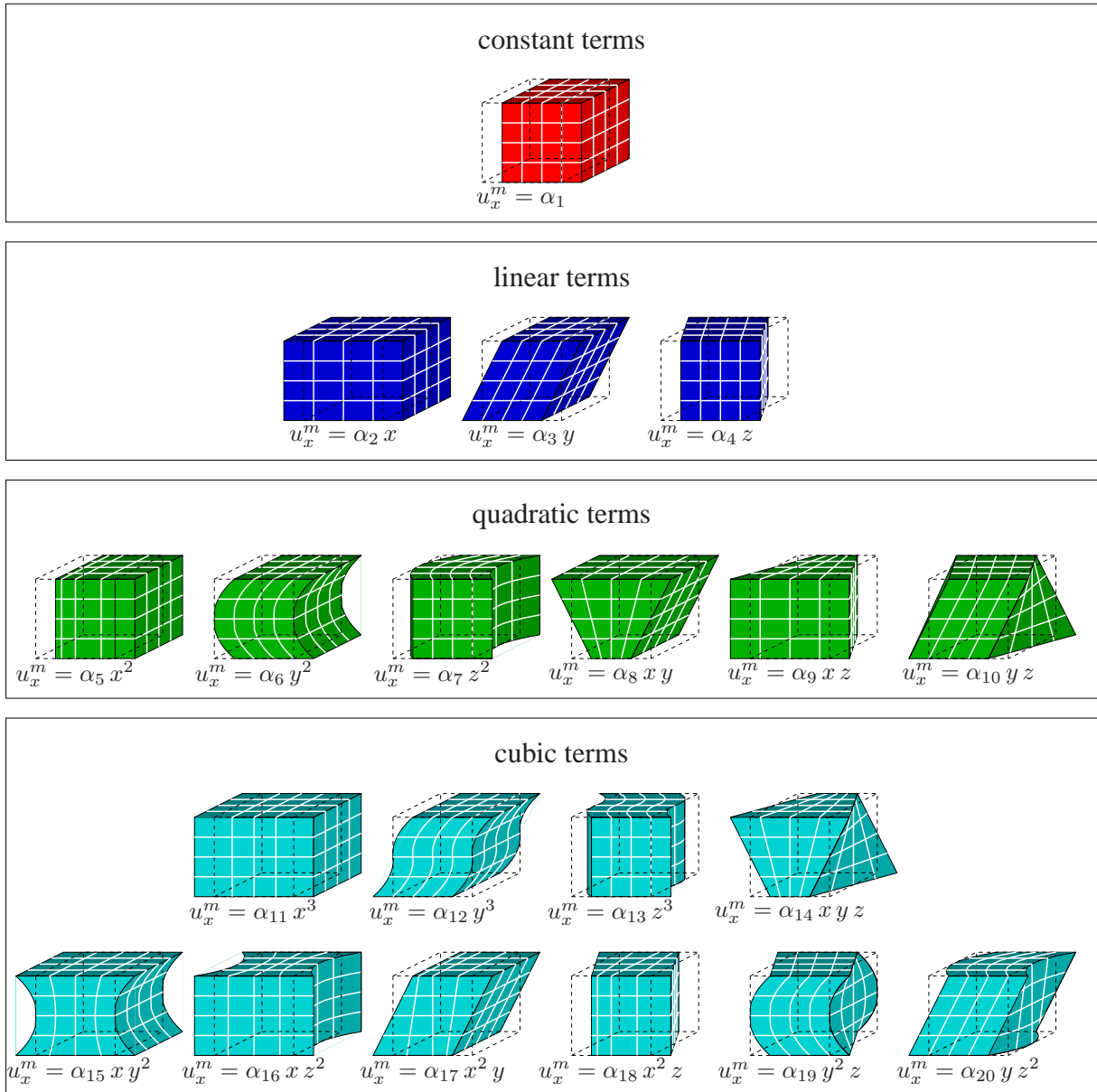


Figure 2: Deformation modes in  $e_x$ -direction up to terms of order three

<sup>2</sup>The Boltzmann continuum theory is the classical continuum theory with three degrees of freedom at the material point. According to the balance of moment of momentum the stress tensor is symmetric.

### 3 Macroscopical Deformation

Within continuum theories, only energy consuming deformation modes are of interest. The deformation modes without consuming energy are the rigid body modes, namely the rigid body translation and the rigid body rotation. These deformation modes have to be eliminated from the Taylor series expansion because they cannot be corresponding candidates for macroscopical deformation modes always consuming energy.

It is obvious that the rigid body displacement is represented by the constant terms of the Taylor series expansion. For instance  $\alpha_1 \neq 0$  yields a horizontal rigid body displacement according to the frame of reference presented in Figure 1. Eliminating all rigid body displacement modes can be done by the restriction

$$\alpha_1 = \beta_1 = \gamma_1 = 0. \quad (2)$$

The rigid body rotations cannot be detected directly, because a superposition of terms of the Taylor series expansion is needed to identify these modes. Using a geometrical approach, the rotation  $\varphi^m(\mathbf{x}, t)$  of the displacement field  $\mathbf{u}^m(\mathbf{x}, t)$  can be calculated by

$$\varphi^m(\mathbf{x}, t) = \frac{1}{2} \text{rot } \mathbf{u}^m(\mathbf{x}, t). \quad (3)$$

In the case of a rigid body rotation mode,  $\varphi^m(\mathbf{x}, t)$  has to be constant but not equal to zero. Thus, while the "rot" operator has involved only first derivatives, the terms of interest have to be linear. Inserting linear terms  $\mathbf{u}^{m,lin}(\mathbf{x}, t)$  of the displacement in eq. (3) yields the constant rotation field  $\varphi^{m,con}(\mathbf{x}, t)$

$$\varphi^{m,con}(\mathbf{x}, t) = \frac{1}{2}(\gamma_3 - \beta_4) \mathbf{e}_x + \frac{1}{2}(\alpha_4 - \gamma_2) \mathbf{e}_y + \frac{1}{2}(\beta_2 - \alpha_3) \mathbf{e}_z. \quad (4)$$

That means that a rigid body rotation appears if  $\gamma_3 \neq \beta_4$ ,  $\alpha_4 \neq \gamma_2$  or  $\beta_2 \neq \alpha_3$ . As a consequence the condition for the elimination of rigid body rotations is

$$\begin{aligned} \gamma_3 &= \beta_4, \\ \alpha_4 &= \gamma_2, \\ \beta_2 &= \alpha_3. \end{aligned} \quad (5)$$

Thus, using a geometrical interpretation of the linear terms, they have to be symmetric while the skew symmetric part has to vanish, which can be formulated using index notation by

$$u_i^{m,lin}(\mathbf{x}, t) \mathbf{e}_j = u_j^{m,lin}(\mathbf{x}, t) \mathbf{e}_i \quad (6)$$

whereby  $u_i^{m,lin}(\mathbf{x}, t)$  are the coefficients of the displacement vector  $\mathbf{u}^{m,lin}(\mathbf{x}, t)$ .

The split into symmetric and skew symmetric part is visualised in Figure 3 for the linear shear deformation modes within the  $\mathbf{e}_x$ - $\mathbf{e}_y$  plane.

Considering the restrictions from the rigid body motion, the remaining microscopical deformation modes can now be related to the macroscopic deformation modes of several continuum theories. This will be done in the following for each continuum theory separately.

#### 3.1 Boltzmann Continuum Theory

Within the standard Boltzmann continuum theory, the linearised strain tensor  $\varepsilon(\mathbf{x}, t)$  is calculated directly from the displacement field  $\mathbf{u}(\mathbf{x}, t)$  by

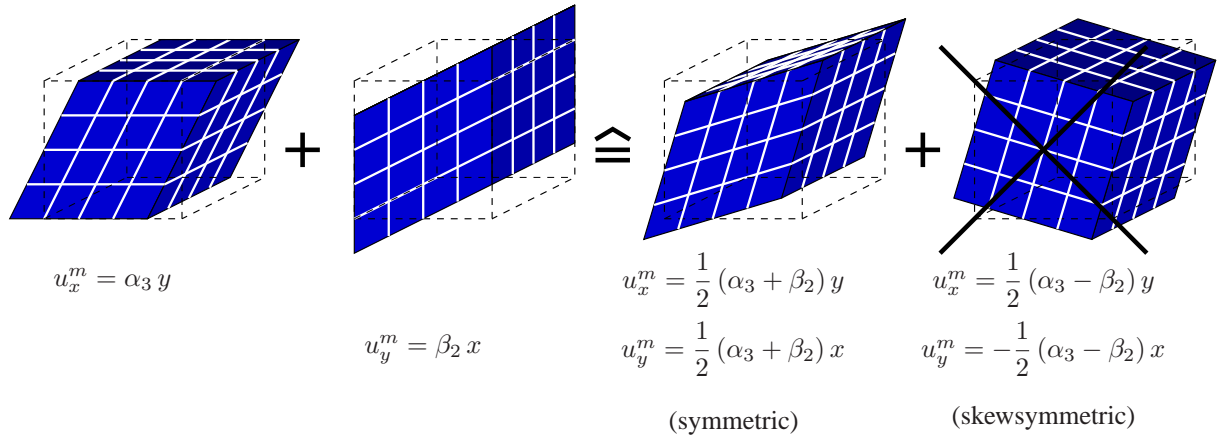


Figure 3: Split of shear mode into symmetric and skew symmetric part

$$\boldsymbol{\varepsilon}(\mathbf{x}, t) = \frac{1}{2} (\text{grad } \mathbf{u}(\mathbf{x}, t) + \text{grad}^T \mathbf{u}(\mathbf{x}, t)). \quad (7)$$

Calculating the right hand term "grad  $\mathbf{u}(\mathbf{x}, t)$ " of eq. (7) by inserting the Taylor series expansion of the displacement field  $\mathbf{u}^m(\mathbf{x}, t)$  according to eq. (1) yields

$$\begin{aligned} \text{grad}(\mathbf{u}^m(\mathbf{x}, t)) = & (\alpha_2 + 2\alpha_5 x + \dots) \mathbf{e}_x \otimes \mathbf{e}_x + (\alpha_3 + 2\alpha_6 y + \dots) \mathbf{e}_x \otimes \mathbf{e}_y + (\alpha_4 + 2\alpha_7 z + \dots) \mathbf{e}_x \otimes \mathbf{e}_z + \\ & (\beta_2 + 2\beta_5 x + \dots) \mathbf{e}_y \otimes \mathbf{e}_x + (\beta_3 + 2\beta_6 y + \dots) \mathbf{e}_y \otimes \mathbf{e}_y + (\beta_4 + 2\beta_7 z + \dots) \mathbf{e}_y \otimes \mathbf{e}_z + \\ & (\gamma_2 + 2\gamma_5 x + \dots) \mathbf{e}_z \otimes \mathbf{e}_x + (\gamma_3 + 2\gamma_6 y + \dots) \mathbf{e}_z \otimes \mathbf{e}_y + (\gamma_4 + 2\gamma_7 z + \dots) \mathbf{e}_z \otimes \mathbf{e}_z \end{aligned} \quad (8)$$

for the microscopical displacement gradient distribution. The macroscopical counterpart can be calculated by taking the volume average of the microscopical distribution. The volume average is defined by

$$\langle \bullet \rangle = \frac{1}{V} \int_{\Omega} (\bullet) dv, \quad (9)$$

whereby  $V$  is the volume of the TVE.

Assuming that the TVE deforms homogeneously and that the TVE has the shape of a cuboid, terms of odd order vanish due to symmetry when the volume average of the microscopical strain distribution is computed

$$\frac{1}{V} \int_{\Omega} A x^n dv = \frac{1}{V} \int_{\Omega} A y^n dv = \frac{1}{V} \int_{\Omega} A z^n dv = 0 \quad \text{with} \quad n = 1, 3, 5, \dots, \quad (10)$$

whereby  $A$  is a coordinate independent coefficient. Keeping in mind that we have introduced a barycentric frame of reference within the TVE, the linear terms would always vanish without any requirement on symmetry. However, this does not hold in general for higher order terms of odd order.

Thus, calculating the macroscopical displacement gradient

$$(\text{grad } \mathbf{u}(\mathbf{x}, t))^M = \langle \text{grad } \mathbf{u}^m(\mathbf{x}, t) \rangle \quad (11)$$

by volume averaging of the microscopical displacement gradient yields

$$\begin{aligned}
(\text{grad } \mathbf{u}(\mathbf{x}, t))^M = & (\alpha_2 + \frac{1}{4} \alpha_{11} b^2 + \frac{1}{12} \alpha_{16} d^2 + \frac{1}{12} \alpha_{17} h^2 + \dots) \mathbf{e}_x \otimes \mathbf{e}_x + \\
& (\alpha_3 + \frac{1}{4} \alpha_{12} h^2 + \frac{1}{12} \alpha_{14} b^2 + \frac{1}{12} \alpha_{18} d^2 + \dots) \mathbf{e}_x \otimes \mathbf{e}_y + \\
& (\alpha_4 + \frac{1}{4} \alpha_{13} d^2 + \frac{1}{12} \alpha_{15} h^2 + \frac{1}{12} \alpha_{19} b^2 + \dots) \mathbf{e}_x \otimes \mathbf{e}_z + \\
& (\beta_2 + \frac{1}{4} \beta_{11} b^2 + \frac{1}{12} \beta_{16} d^2 + \frac{1}{12} \beta_{17} h^2 + \dots) \mathbf{e}_y \otimes \mathbf{e}_x + \\
& (\beta_3 + \frac{1}{4} \beta_{12} h^2 + \frac{1}{12} \beta_{14} b^2 + \frac{1}{12} \beta_{18} d^2 + \dots) \mathbf{e}_y \otimes \mathbf{e}_y + \\
& (\beta_4 + \frac{1}{4} \beta_{13} d^2 + \frac{1}{12} \beta_{15} h^2 + \frac{1}{12} \beta_{19} b^2 + \dots) \mathbf{e}_y \otimes \mathbf{e}_z + \\
& (\gamma_2 + \frac{1}{4} \gamma_{11} b^2 + \frac{1}{12} \gamma_{16} d^2 + \frac{1}{12} \gamma_{17} h^2 + \dots) \mathbf{e}_z \otimes \mathbf{e}_x + \\
& (\gamma_3 + \frac{1}{4} \gamma_{12} h^2 + \frac{1}{12} \gamma_{14} b^2 + \frac{1}{12} \gamma_{18} d^2 + \dots) \mathbf{e}_z \otimes \mathbf{e}_y + \\
& (\gamma_4 + \frac{1}{4} \gamma_{13} d^2 + \frac{1}{12} \gamma_{15} h^2 + \frac{1}{12} \gamma_{19} b^2 + \dots) \mathbf{e}_z \otimes \mathbf{e}_z
\end{aligned} \tag{12}$$

whereby  $b$  is the width of the TVE into  $\mathbf{e}_x$ -direction,  $d$  the height into  $\mathbf{e}_y$ -direction, and  $h$  the thickness in the direction of depth  $\mathbf{e}_z$  as shown in Figure 1.

There are different approaches to reduce the number of terms in eq. (12), however, all of them yield the same result. The simplest approach is the consideration that the material body is intended to have an infinitesimally small extension, thus the dimensions  $b$ ,  $d$  and  $h$  tend to zero. The second approach is the *a priori* assumption that only terms of linear order may be reflected by the Boltzmann continuum theory, and therefore setting all coefficients of the higher order terms to zero. The third approach can be carried out by making numerical experiments for the TVE: for a fixed macroscopical displacement gradient, e. g.,  $\alpha_2 = \frac{1}{4} \alpha_{11} b^2 = \frac{1}{12} \alpha_{16} d^2 = \frac{1}{12} \alpha_{17} h^2 = \dots = \text{constant}$ , the energy needed to achieve the deformed configuration can be calculated using a linear elastic material law. However, the numerical results (shown in Section 4) demonstrate, that the term of lowest order always needs the lowest energy. Looking for the energetical minimum to achieve the equilibrium state, the term of lowest order is taken as the winning term chosen to reflect the macroscopic deformation. As mentioned before, all three approaches lead to the same reduction of the macroscopical displacement gradient

$$\begin{aligned}
(\text{grad } \mathbf{u}(\mathbf{x}, t))^{M,red} = & \alpha_2 \mathbf{e}_x \otimes \mathbf{e}_x + \alpha_3 \mathbf{e}_x \otimes \mathbf{e}_y + \alpha_4 \mathbf{e}_x \otimes \mathbf{e}_z + \\
& \beta_2 \mathbf{e}_y \otimes \mathbf{e}_x + \beta_3 \mathbf{e}_y \otimes \mathbf{e}_y + \beta_4 \mathbf{e}_y \otimes \mathbf{e}_z + \\
& \gamma_2 \mathbf{e}_z \otimes \mathbf{e}_x + \gamma_3 \mathbf{e}_z \otimes \mathbf{e}_y + \gamma_4 \mathbf{e}_z \otimes \mathbf{e}_z.
\end{aligned} \tag{13}$$

Inserting this reduced macroscopical displacement gradient into eq. (7) yields the relation of interest between macroscopical deformation  $\varepsilon^M$  and microscopical deformation represented by the Taylor series expansion

$$\varepsilon^M = \alpha_2 \mathbf{e}_x \otimes \mathbf{e}_x + \alpha_3 \mathbf{e}_x \otimes \mathbf{e}_y + \alpha_4 \mathbf{e}_x \otimes \mathbf{e}_z + \beta_2 \mathbf{e}_y \otimes \mathbf{e}_x + \beta_3 \mathbf{e}_y \otimes \mathbf{e}_y + \beta_4 \mathbf{e}_y \otimes \mathbf{e}_z + \gamma_2 \mathbf{e}_z \otimes \mathbf{e}_x + \gamma_3 \mathbf{e}_z \otimes \mathbf{e}_y + \gamma_4 \mathbf{e}_z \otimes \mathbf{e}_z \tag{14}$$

whereby the symmetry condition of the strain tensor is already fulfilled by the restrictions from excluding rigid body rotations according to eq. (5). That means that the six independent entries of the strain tensor directly correspond to the six linear deformation modes of the Taylor series expansion (originally 9 linear terms minus 3 rigid body rotation constraints).

### 3.2 Second Gradient Theory

In the case of the second gradient theory not only the gradient of the displacement field is considered (eq. (7)), but in addition to this also the second gradient  $\kappa$  is regarded as a strain-like quantity

$$\kappa = \text{grad}(\text{grad } \mathbf{u}). \tag{15}$$

Inserting the displacement field in the form of the Taylor series expansion into the right hand side of eq. (15) yields

$$\begin{aligned}
\text{grad}(\text{grad} \mathbf{u}^m(\mathbf{x}, t)) = & (2\alpha_5 + 6\alpha_{11}x + \dots) \mathbf{e}_x \otimes \mathbf{e}_x \otimes \mathbf{e}_x + (\alpha_8 + 2\alpha_{14}x + \dots) \mathbf{e}_x \otimes \mathbf{e}_x \otimes \mathbf{e}_y + \\
& (\alpha_{10} + 2\alpha_{16}x + \dots) \mathbf{e}_x \otimes \mathbf{e}_x \otimes \mathbf{e}_z + (\alpha_8 + 2\alpha_{14}x + \dots) \mathbf{e}_x \otimes \mathbf{e}_y \otimes \mathbf{e}_x + \\
& (2\alpha_6 + 6\alpha_{12}y + \dots) \mathbf{e}_x \otimes \mathbf{e}_y \otimes \mathbf{e}_y + (\alpha_9 + 2\alpha_{15}y + \dots) \mathbf{e}_x \otimes \mathbf{e}_y \otimes \mathbf{e}_z + \\
& (\alpha_{10} + 2\alpha_{16}x + \dots) \mathbf{e}_x \otimes \mathbf{e}_z \otimes \mathbf{e}_x + (\alpha_9 + 2\alpha_{15}y + \dots) \mathbf{e}_x \otimes \mathbf{e}_z \otimes \mathbf{e}_y + \\
& (2\alpha_7 + 6\alpha_{13}z + \dots) \mathbf{e}_x \otimes \mathbf{e}_z \otimes \mathbf{e}_z + (2\beta_5 + 6\beta_{11}x + \dots) \mathbf{e}_x \otimes \mathbf{e}_x \otimes \mathbf{e}_x + \\
& (\beta_8 + 2\beta_{14}x + \dots) \mathbf{e}_x \otimes \mathbf{e}_x \otimes \mathbf{e}_y + (\beta_{10} + 2\beta_{16}x + \dots) \mathbf{e}_x \otimes \mathbf{e}_x \otimes \mathbf{e}_z + \\
& (\beta_8 + 2\beta_{14}x + \dots) \mathbf{e}_x \otimes \mathbf{e}_y \otimes \mathbf{e}_x + (2\beta_6 + 6\beta_{12}y + \dots) \mathbf{e}_x \otimes \mathbf{e}_y \otimes \mathbf{e}_y + \\
& (\beta_9 + 2\beta_{15}y + \dots) \mathbf{e}_x \otimes \mathbf{e}_y \otimes \mathbf{e}_z + (\beta_{10} + 2\beta_{16}x + \dots) \mathbf{e}_x \otimes \mathbf{e}_z \otimes \mathbf{e}_x + \\
& (\beta_9 + 2\beta_{15}y + \dots) \mathbf{e}_x \otimes \mathbf{e}_z \otimes \mathbf{e}_y + (2\beta_7 + 6\beta_{13}z + \dots) \mathbf{e}_x \otimes \mathbf{e}_z \otimes \mathbf{e}_z + \\
& (2\gamma_5 + 6\gamma_{11}x + \dots) \mathbf{e}_x \otimes \mathbf{e}_x \otimes \mathbf{e}_x + (\gamma_8 + 2\gamma_{14}x + \dots) \mathbf{e}_x \otimes \mathbf{e}_x \otimes \mathbf{e}_y + \\
& (\gamma_{10} + 2\gamma_{16}x + \dots) \mathbf{e}_x \otimes \mathbf{e}_x \otimes \mathbf{e}_z + (\gamma_8 + 2\gamma_{14}x + \dots) \mathbf{e}_x \otimes \mathbf{e}_y \otimes \mathbf{e}_x + \\
& (2\gamma_6 + 6\gamma_{12}y + \dots) \mathbf{e}_x \otimes \mathbf{e}_y \otimes \mathbf{e}_y + (\gamma_9 + 2\gamma_{15}y + \dots) \mathbf{e}_x \otimes \mathbf{e}_y \otimes \mathbf{e}_z + \\
& (\gamma_{10} + 2\gamma_{16}x + \dots) \mathbf{e}_x \otimes \mathbf{e}_z \otimes \mathbf{e}_x + (\gamma_9 + 2\gamma_{15}y + \dots) \mathbf{e}_x \otimes \mathbf{e}_z \otimes \mathbf{e}_y + \\
& (2\gamma_7 + 6\gamma_{13}z + \dots) \mathbf{e}_x \otimes \mathbf{e}_z \otimes \mathbf{e}_z
\end{aligned} \tag{16}$$

for the microscopical second gradient of the displacement field. The macroscopical second gradient again can be calculated by taking the volume average (eq. (9)) of the microscopical distribution

$$(\text{grad}(\text{grad} \mathbf{u}(\mathbf{x}, t)))^M = \langle \text{grad}(\text{grad} \mathbf{u}^m(\mathbf{x}, t)) \rangle. \tag{17}$$

Using the same assumptions as before in the case of the Boltzmann continuum (cuboid shape of homogeneous TVE) in connection with the considerations reducing the number of terms (small size of TVE or a priori restriction to quadratic terms now or energetical considerations), the macroscopic curvature tensor in dependence of the coefficients of the Taylor series expansion is found to be

$$\begin{aligned}
\boldsymbol{\kappa}^M = & 2\alpha_5 \mathbf{e}_x \otimes \mathbf{e}_x \otimes \mathbf{e}_x + \alpha_8 \mathbf{e}_x \otimes \mathbf{e}_x \otimes \mathbf{e}_y + \alpha_{10} \mathbf{e}_x \otimes \mathbf{e}_x \otimes \mathbf{e}_z + \alpha_8 \mathbf{e}_x \otimes \mathbf{e}_y \otimes \mathbf{e}_x + \\
& 2\alpha_6 \mathbf{e}_x \otimes \mathbf{e}_y \otimes \mathbf{e}_y + \alpha_9 \mathbf{e}_x \otimes \mathbf{e}_y \otimes \mathbf{e}_z + \alpha_{10} \mathbf{e}_x \otimes \mathbf{e}_z \otimes \mathbf{e}_x + \alpha_9 \mathbf{e}_x \otimes \mathbf{e}_z \otimes \mathbf{e}_y + \\
& 2\alpha_7 \mathbf{e}_x \otimes \mathbf{e}_z \otimes \mathbf{e}_z + 2\beta_5 \mathbf{e}_x \otimes \mathbf{e}_x \otimes \mathbf{e}_x + \beta_8 \mathbf{e}_x \otimes \mathbf{e}_x \otimes \mathbf{e}_y + \beta_{10} \mathbf{e}_x \otimes \mathbf{e}_x \otimes \mathbf{e}_z + \\
& \beta_8 \mathbf{e}_x \otimes \mathbf{e}_y \otimes \mathbf{e}_x + 2\beta_6 \mathbf{e}_x \otimes \mathbf{e}_y \otimes \mathbf{e}_y + \beta_9 \mathbf{e}_x \otimes \mathbf{e}_y \otimes \mathbf{e}_z + \beta_{10} \mathbf{e}_x \otimes \mathbf{e}_z \otimes \mathbf{e}_x + \\
& \beta_9 \mathbf{e}_x \otimes \mathbf{e}_z \otimes \mathbf{e}_y + 2\beta_7 \mathbf{e}_x \otimes \mathbf{e}_z \otimes \mathbf{e}_z + 2\gamma_5 \mathbf{e}_x \otimes \mathbf{e}_x \otimes \mathbf{e}_x + \gamma_8 \mathbf{e}_x \otimes \mathbf{e}_x \otimes \mathbf{e}_y + \\
& \gamma_{10} \mathbf{e}_x \otimes \mathbf{e}_x \otimes \mathbf{e}_z + \gamma_8 \mathbf{e}_x \otimes \mathbf{e}_y \otimes \mathbf{e}_x + 2\gamma_6 \mathbf{e}_x \otimes \mathbf{e}_y \otimes \mathbf{e}_y + \gamma_9 \mathbf{e}_x \otimes \mathbf{e}_y \otimes \mathbf{e}_z + \\
& \gamma_{10} \mathbf{e}_x \otimes \mathbf{e}_z \otimes \mathbf{e}_x + \gamma_9 \mathbf{e}_x \otimes \mathbf{e}_z \otimes \mathbf{e}_y + 2\gamma_7 \mathbf{e}_x \otimes \mathbf{e}_z \otimes \mathbf{e}_z .
\end{aligned} \tag{18}$$

Due to Clairaut's theorem (also called Schwarz's theorem) this tensor of third order is symmetric with respect to the second and third base system. Thus, from the 27 overall coefficients only 18 are independent, which directly correspond to the 18 independent quadratic terms of the Taylor series expansion.

### 3.3 MMM Theories

A completely different approach is chosen to identify the according terms of the Taylor series expansion within the MMM theories, which means the micromorphic continuum theory and the restrictive special cases. Based on the assumption that the extra deformation is strongly related to the macroscopic deformation, the appropriate modes of the expansion can be selected being able to reflect this extra deformation. To be more specific: the extra stretch deformation, called (directional) microstretch, should also represent directional volumetric deformation like the macroscopic stretch mode, but it should be of course independent of the macroscopic mode. The same holds for the extra shear mode called microshear and the extra rotation called micropolar deformation.

A non-homogeneous extra stretch into horizontal direction can be represented by the terms  $u_x^m = \alpha_{11}x^3$ ,  $u_x^m = \alpha_{15}xy^2$  and  $u_x^m = \alpha_{16}xz^2$ . However, splitting the second and third term into a volumetric and a deviatoric part, only the volumetric part is able to represent the directional microstretch. The remaining modes being able to reflect microstretch into horizontal direction are presented in Figure 4.

An energy criterion is used to select from the available modes that one which will reflect the extra stretch deformation. To make the modes presented in Figure 4 comparable, the coefficients  $\alpha_i$  are chosen in such a way, that

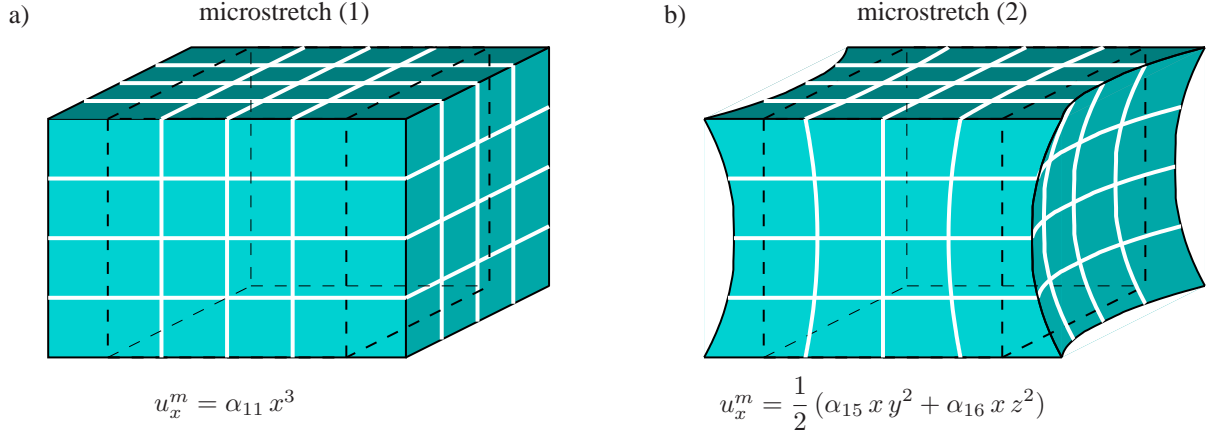


Figure 4: possible deformation modes reflecting microstretch into horizontal direction

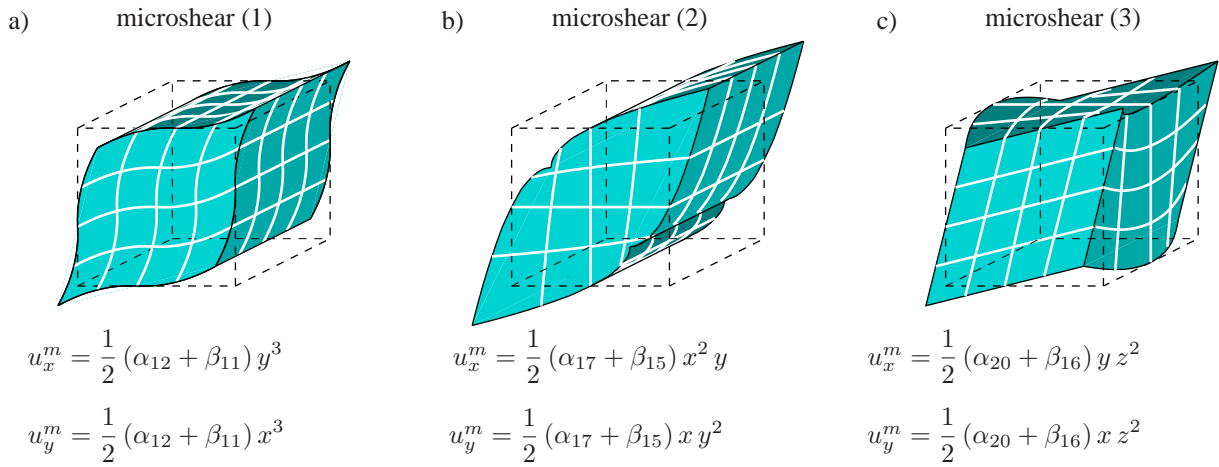


Figure 5: possible deformation modes reflecting microshear within the  $\mathbf{e}_x/\mathbf{e}_y$ -plane

the macroscopic stretch derived by calculating the volume average of the local stretch distribution is equal for both modes. Calculation of the energy using a Finite Element (FE) code shows, that the mode on the left of Figure 4 is about two times stiffer than the mode on the right. Of course, this depends on the chosen material parameters, especially on the relation between stiffness with respect to stretch and shear, but for a realistic set of material parameters the left one will always be stiffer. Thus, looking for the energetical minimum to deform the TVE, the deformation mode on the right hand side of Figure 4 is chosen to reflect the directional microstretch.

Analogously the same can be done for the microshear. Looking at terms able to represent a shear deformation within the  $\mathbf{e}_x/\mathbf{e}_y$ -plane, which is not identical to the macroscopic shear deformation, one finds the terms visualised in Figure 5.

Again the energy criterion is used to choose the inhomogeneous deformation mode consuming the lowest amount of energy as the deformation mode reflecting microshear. Thereby, to make the deformation modes comparable, they are normalised in such a way that the macroscopic shear deformation calculated by the volume average of the local distribution is equal for the different modes. FE calculations show that the first and third mode presented in Figure 5 are about 1.5 times stiffer than the second mode, so that the second one is chosen to reflect the microshear deformation.

Finally, this approach is also carried out for the micropolar deformation. The deformation modes reflecting micropolar deformations should be closely related to the skew symmetric macroscopic shear deformation, whereby it does not matter that this is a rigid body mode. The modes reflecting this rotational effect and being independent of the macroscopic skew symmetric shear mode are presented in Figure 6.

Performing a FE analysis to determine the energy needed for the deformation, whereby the modes are now normalised so that the macroscopic skew symmetric shear deformation calculated by the volume average of the local distribution is equal for the three modes presented in Figure 6, the second mode of Figure 6 is about two times

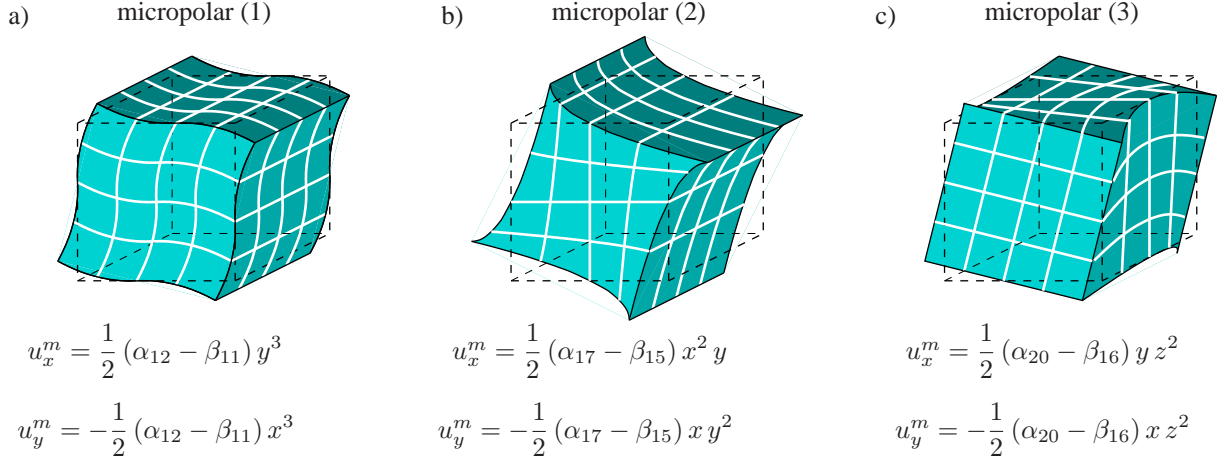


Figure 6: possible deformation modes reflecting micropolar deformation within the  $\mathbf{e}_x/\mathbf{e}_y$ -plane

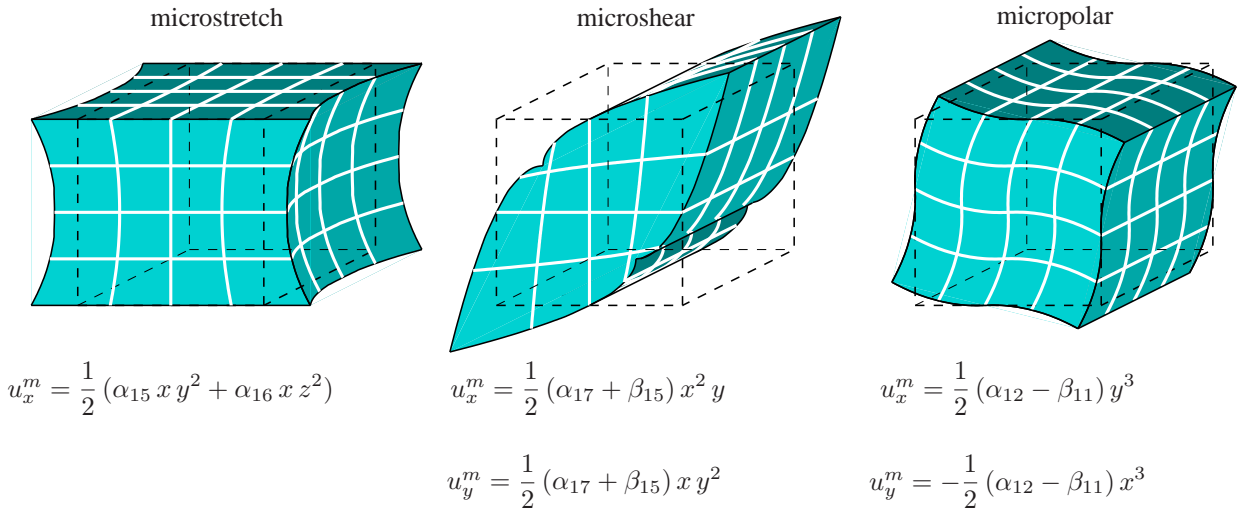


Figure 7: modes reflecting micromorphic extra deformation

stiffer than the first one, while the third one is about three times stiffer than the first one. Thus, the first one is chosen as the mode reflecting the micropolar deformation.

Comparing the underlying terms used for the representation of the microshear and micropolar deformation, it is interesting, that they are not based on the same terms of the Taylor series expansion in terms of the symmetric part reflecting the microshear deformation and the skew symmetric part reflecting the micropolar deformation.

Figure 7 shows an overview of the extra deformation modes used in the following to reflect the extra higher order deformation within the micromorphic continuum theory with the restrictions due to symmetry of the microshear mode and skew symmetry of the micropolar mode

$$\alpha_{17} = \beta_{15} \quad \text{and} \quad \alpha_{12} = -\beta_{11}. \quad (19)$$

Within the micromorphic continuum theory these higher order modes are reformulated by a total of 9 independent variables. Using these variables in addition to the displacement field  $\mathbf{u}$  as the master field within a FE formulation, also the gradient of the independent variables has to exist. For the present approach that means, that also the gradient of the micromorphic deformation modes has to be provided by the Taylor series expansion.

The simplest way to generate the required gradient modes is by integration of the higher order modes into the several directions, which yields terms of fourth order. The results are presented in Table 1 for the microstretch mode, in Table 2 for the microshear mode, and in Table 3 for the micropolar deformation. Thereby, utilising the symmetry and skew symmetry of the modes, the terms are expressed using new scaling factors  $\alpha_i$ .

microstretch mode:	$u_x^m = \alpha_A (x y^2 + x z^2)$
gradient mode into $\mathbf{e}_x$ -direction:	$u_x^m = \alpha_B (\frac{1}{2} x^2 y^2 + \frac{1}{2} x^2 z^2)$
gradient mode into $\mathbf{e}_y$ -direction:	$u_x^m = \alpha_C (\frac{1}{3} x y^3 + x y z^2)$
gradient mode into $\mathbf{e}_z$ -direction:	$u_x^m = \alpha_D (x y^2 z + \frac{1}{3} x z^3)$

Table 1: gradient modes of horizontal microstretch

microshear mode:	$u_x^m = \alpha_E x^2 y$	$u_y^m = \alpha_E x y^2$
gradient mode into $\mathbf{e}_x$ -direction:	$u_x^m = \alpha_F \frac{1}{3} x^3 y$	$u_y^m = \alpha_F \frac{1}{2} x^2 y^2$
gradient mode into $\mathbf{e}_y$ -direction:	$u_x^m = \alpha_G \frac{1}{2} x^2 y^2$	$u_y^m = \alpha_G \frac{1}{3} x y^3$
gradient mode into $\mathbf{e}_z$ -direction:	$u_x^m = \alpha_H x^2 y z$	$u_y^m = \alpha_H x y^2 z$

Table 2: gradient modes of microshear within the  $\mathbf{e}_x/\mathbf{e}_y$ -plane

micropolar mode:	$u_x^m = \alpha_I y^3$	$u_y^m = -\alpha_I x^3$
gradient mode into $\mathbf{e}_x$ -direction:	$u_x^m = \alpha_J x y^3$	$u_y^m = -\alpha_J \frac{1}{4} x^4$
gradient mode into $\mathbf{e}_y$ -direction:	$u_x^m = \alpha_K \frac{1}{4} y^4$	$u_y^m = -\alpha_K x^3 y$
gradient mode into $\mathbf{e}_z$ -direction:	$u_x^m = \alpha_L y^3 z$	$u_y^m = -\alpha_L x^3 z$

Table 3: gradient modes of micropolar deformation within the  $\mathbf{e}_x/\mathbf{e}_y$ -plane

At the moment, terms of second order are not used to represent a micromorphic continuum. However, the terms of second order are able to describe similar effects as the terms of fourth order. While the terms of second order describe the gradient of the macroscopic first order terms, the fourth order terms describe the gradient of the microscopic third order terms. Thus, instead of using fourth order terms to describe the gradient of micromorphic micromotion, the second order terms may be used without changing the overall behaviour. This is in good agreement with the energy criterion used before for the selection of micromorphic modes: the energy per volume (and therefore also the stiffness) of the second order terms increases quadratically with the size of the TVE while the energy per volume of the fourth order terms increases quartically with the size in the case of a homogeneous TVE. That means that comparing modes of second order and fourth order describing the same gradient-like effect, the second order terms behave much softer in the case of a homogeneous TVE. The second order gradient modes can be generated by integration of the macroscopic deformation modes into the several directions. Thereby it does not matter that the macroscopic skew symmetric shear mode has to be integrated, because the skew symmetric shear is indeed a zero energy mode, but the integrated second order modes are not zero energy modes. The integrated modes derived from macroscopic (linear) deformation modes are presented in Tables 4, 5 and 6.

Only 18 independent modes of second order are available. Thus, the calculated gradient modes of second order are not linearly independent. E. g., superposition of gradient modes of macroshear and skew symmetric shear mode into  $\mathbf{e}_1$ -direction yields the gradient mode of the macrostretch into  $\mathbf{e}_2$ -direction. In principle two gradients can be of second order terms while the third one has to be of fourth order to guarantee independency. There is no special argument to take a certain set of gradient modes as the third possible mode, which means as that one with terms of fourth order. However, it seems to be reasonable to take into account the gradient modes of the macrostretch mode, so that there is no a priori coupling between displacements into  $\mathbf{e}_1$ -direction and displacements into  $\mathbf{e}_2$ -direction. Furthermore, this has the advantage, that again an energy criterion can be used to decide whether the terms of second order represent the macroshear mode or the gradient modes of the skew symmetric shear mode. Due to the relationship between the macroscopic symmetric and skew symmetric modes, for fixed  $\alpha_i$  the modes

macrostretch mode:	$u_x^m = \alpha_A x$
gradient mode into $\mathbf{e}_x$ -direction:	$u_x^m = \alpha_B \frac{1}{2} x^2$
gradient mode into $\mathbf{e}_y$ -direction:	$u_x^m = \alpha_C x y$
gradient mode into $\mathbf{e}_z$ -direction:	$u_x^m = \alpha_D x z$

Table 4: gradient modes of horizontal macrostretch

macroshear mode:	$u_x^m = \alpha_E y$	$u_y^m = \alpha_E x$
gradient mode into $\mathbf{e}_x$ -direction:	$u_x^m = \alpha_F x y$	$u_y^m = \alpha_F \frac{1}{2} x^2$
gradient mode into $\mathbf{e}_y$ -direction:	$u_x^m = \alpha_G \frac{1}{2} y^2$	$u_y^m = \alpha_G x y$
gradient mode into $\mathbf{e}_z$ -direction:	$u_x^m = \alpha_H y z$	$u_y^m = \alpha_H x z$

Table 5: gradient modes of macroshear within the  $\mathbf{e}_x/\mathbf{e}_y$ -plane

skew symmetric shear mode:	$u_x^m = \alpha_I y$	$u_y^m = -\alpha_I x$
gradient mode into $\mathbf{e}_x$ -direction:	$u_x^m = \alpha_J x y$	$u_y^m = -\alpha_J \frac{1}{2} x^2$
gradient mode into $\mathbf{e}_y$ -direction:	$u_x^m = \alpha_K \frac{1}{2} y^2$	$u_y^m = -\alpha_K x y$
gradient mode into $\mathbf{e}_z$ -direction:	$u_x^m = \alpha_L y z$	$u_y^m = -\alpha_L x z$

Table 6: gradient modes of skew symmetric shear deformation within the  $\mathbf{e}_x/\mathbf{e}_y$ -plane

are comparable. Thus, within a FE analysis the energy for the gradient modes according to the symmetric and skew symmetric part can be calculated. The results show that the gradient modes according to the symmetric part are always stiffer than the modes according to the skew symmetric part. As a consequence modes of second order are used to represent the gradient of the micropolar deformation while terms of fourth order are used to represent the gradient of the microshear deformation.

Up to now the presented approach is restricted to qualitative results describing the relation between certain modes of the Taylor series expansion. For quantitative results an explicit reformulation of the deformation modes is needed. This step of reformulation is independent of the previous step of mode selection. Thus, there is again a lot of freedom to choose an appropriate rule for the reformulation in the form of new independent variables. The rule presented in the following is only one possible choice among others.

Keeping in mind that the micromorphic deformation modes consisting of the directional microstretch, the microshear and the micropolar deformation are all of third order, a very simple rule for the reformulation can be used, which is

$$\mathbf{A} = u_{a,bbc}^m \mathbf{e}_a \otimes \mathbf{e}_c \quad (20)$$

yielding the micromotion tensor with 9 independent coefficients. The rule furthermore guarantees that the micromotion vanishes for modes of order lower than 3, and that the micromotion itself also vanishes for modes of fourth order taking the volume average (again under assumption of a cuboid symmetric TVE). For the representation of the micromotion modes of second order as well as modes of fourth order are used. Therefore, the integrated modes of fourth order can not be used directly. The reformulation rule may use only second derivatives. The simplest version of the rule is

$$\overset{3}{\mathbf{B}} = u_{a,bc}^m \mathbf{e}_a \otimes \mathbf{e}_b \otimes \mathbf{e}_c. \quad (21)$$

However, this rule is not able to represent the gradient completely due to the symmetry with respect to the second and third base system, i. e., it yields only 18 independent coefficients while 27 are needed. This strong coupling by Clairaut's theorem has to be circumvented. This can, e. g., be done by taking the symmetric part of the first derivative only and by calculating the second derivative

$$\overset{3}{\mathbf{C}} = \frac{1}{2} (u_{a,bc}^m + u_{b,ac}^m) \mathbf{e}_a \otimes \mathbf{e}_b \otimes \mathbf{e}_c, \quad (22)$$

which is symmetric with respect to the first and second base system also yielding 18 independent coefficients only. However, by a superposition of both rules, e. g., weighting both rules by a factor of 0.5, a rule is defined which yields the required 27 independent coefficients

$$\overset{3}{\mathbf{D}} = \frac{1}{2} (\overset{3}{\mathbf{B}} + \overset{3}{\mathbf{C}}) = \left( \frac{3}{4} u_{a,bc}^m + \frac{1}{4} u_{b,ac}^m \right) \mathbf{e}_a \otimes \mathbf{e}_b \otimes \mathbf{e}_c, \quad (23)$$

whereby  $\overset{3}{\mathbf{D}}$  represents the gradient of the micromotion  $\overset{3}{\mathbf{A}}$ . The coefficients of  $\overset{3}{\mathbf{D}}$  contain fourth order terms, which still depend on the position within the TVE. To avoid this, the volume average is taken. Finally one gets

$$\overset{3}{\mathbf{D}} = \left\langle \left( \frac{3}{4} u_{a,bc}^m + \frac{1}{4} u_{b,ac}^m \right) \mathbf{e}_a \otimes \mathbf{e}_b \otimes \mathbf{e}_c \right\rangle, \quad (24)$$

which yields non-zero values only for the gradient modes of the micromotion.

In conclusion this approach enables the calculation of the kinematical degrees of freedom based on the Taylor series expansion. Thereby the explicit calculation of the kinematical degrees of freedom may clarify which terms of the expansion are associated with the macrodeformation and microdeformation, respectively. This will be demonstrated on the basis of the simplest restricted micromorphic continuum theory, which is the Cosserat continuum theory.

The linearised Cosserat strain tensor  $\bar{\boldsymbol{\varepsilon}}$  is given by

$$\bar{\boldsymbol{\varepsilon}} = \text{grad } \mathbf{u} + \overset{3}{\mathbf{E}} \cdot \bar{\boldsymbol{\varphi}}, \quad (25)$$

whereby  $\overset{3}{\mathbf{E}}$  is the permutation tensor,  $\mathbf{u}$  the displacement field and  $\bar{\boldsymbol{\varphi}}$  the field of extra-rotations. The terms of the Taylor series expansion needed for the reflection of the complete Cosserat deformation are the linear terms and in addition the micropolar terms including their gradients as given in Table 6

$$\begin{aligned} \mathbf{u}^m(\mathbf{x}, t) = & (\alpha_1 x + \zeta_1 y + \eta_1 z + \zeta_2 y^3 - \eta_2 z^3 + \\ & \zeta_3 x y + \frac{1}{2} \zeta_4 y^2 + \zeta_5 y z - \frac{1}{2} \eta_3 z^2 - \eta_4 x z - \eta_5 y z) \mathbf{e}_x + \\ & (\beta_1 y + \zeta_1 x + \xi_1 z + \xi_2 z^3 - \zeta_2 x^3 + \\ & \xi_3 y z + \frac{1}{2} \xi_4 z^2 + \xi_5 x z - \frac{1}{2} \zeta_3 x^2 - \zeta_4 x y - \zeta_5 x z) \mathbf{e}_y + \\ & (\gamma_1 z + \eta_1 x + \xi_1 y + \eta_2 x^3 - \xi_2 y^3 + \\ & \eta_3 x z + \frac{1}{2} \eta_4 x^2 + \eta_5 x y - \frac{1}{2} \xi_3 y^2 - \xi_4 y z - \xi_5 x y) \mathbf{e}_z. \end{aligned} \quad (26)$$

Compared to eq. 1 the coefficients in eq. 26 are reformulated to include the symmetry and skew symmetry conditions. Thereby the coefficients  $\xi_i$  indicate a deformation mode within the  $\mathbf{e}_y$ - $\mathbf{e}_z$ -plane,  $\eta_i$  within the  $\mathbf{e}_x$ - $\mathbf{e}_z$ -plane, and  $\zeta_i$  within the  $\mathbf{e}_x$ - $\mathbf{e}_y$ -plane.

In a next step the Cosserat strain tensor  $\bar{\boldsymbol{\varepsilon}}$  is set equal to the volume average of the gradient of the displacement field expressed by the Taylor series expansion

$$\bar{\varepsilon} := \langle \text{grad } \mathbf{u}^m(\mathbf{x}, t) \rangle. \quad (27)$$

Thereby the skew symmetric part of the Cosserat strain tensor  $\bar{\varepsilon}$  is reflected by the micropolar deformation. However, there is no possibility to distinguish between the skew symmetric part involved by the gradient of the displacement field and the a priori skew symmetric part due to the extra-rotation  $\bar{\varphi}$ . Thus, the skew symmetric part of the gradient of the displacement field is set to zero. This is in agreement with the consideration that if all micropolar effects vanish, the continuum theory reduces toward the Boltzmann continuum theory, where the strain tensor is symmetric

$$\text{skw } \bar{\varepsilon} := \overset{3}{\mathbf{E}} \cdot \bar{\varphi}. \quad (28)$$

For a homogeneous cuboidal TVE (edge length  $l$ ) the resulting skew symmetric part can be calculated using eq. 25. In a last step the information about the extra-rotation can be extracted from the skew symmetric part using eq. 28, which gives

$$\bar{\varphi} = \frac{1}{4} \xi_2 l^2 \mathbf{e}_x + \frac{1}{4} \eta_2 l^2 \mathbf{e}_y + \frac{1}{4} \zeta_2 l^2 \mathbf{e}_z. \quad (29)$$

#### 4 Application to Microstructures

In the following the presented approach is applied to four different kinds of TVEs as shown in Figure 8. The first one is a homogeneous TVE, the second a plated cross-like TVE assembled by shell elements, the third a cross-like TVE assembled by beam elements, and the last one a TVE which shows a negative radical strain coefficient on the macroscopical level due to the special topology of the microstructure. In the following the last one will be called the star-like TVE. For a better understanding of the mechanism responsible for the negative radical strain coefficient, a two-dimensional sketch is presented on the right hand side of Figure 8. The modes of interest chosen by energetical considerations are applied to these TVEs. By scaling the size of the TVEs it can be observed that the energy per volume increases at different rates for the different modes. This information is used to decide if the deformation mode under consideration may play an important role on a macroscopical level or not: if the energy per volume increases very fast, the TVE is very stiff with respect to the deformation mode, and so the load transfer will be taken by weaker deformation modes consuming less energy.

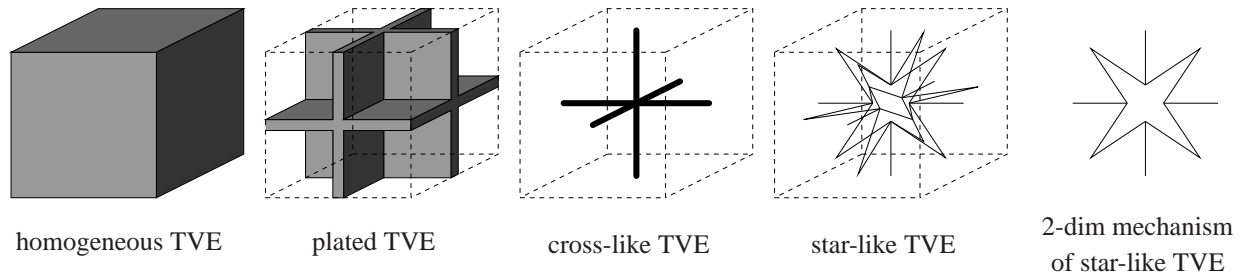


Figure 8: Microstructures under investigation

##### 4.1 Homogeneous TVE

Table 7 shows the deformation modes, which are investigated in the following, and the corresponding numerical results. All further modes not presented in the table can be reconstructed from these modes using the symmetry condition. The fifth up to the ninth column of the table indicate the macroscopic continuum theory the deformation modes belong to. Thereby the following abbreviations are used: BCT (Boltzmann continuum theory), SGT (second gradient theory),  $\mu\text{M}$  (micromorphic theory),  $\mu\text{P}$  (micropolar theory), and  $\mu\text{S}$  (microstretch theory). "X" means that the mode is used directly without any further restriction within a certain continuum theory. "C" means that the mode is used indirectly requiring some extra conditions in the form of a superposition. This applies to the gradient of the micropolar deformation (no. 15), which can also be understood as a superposition of the quadratic modes (no. 3 to 7), and of course vice versa.

no.	$u_x^m = \alpha_i \cdot \dots$	$u_y^m = \alpha_i \cdot \dots$	geometrical Interpretation	BCT	SGT	$\mu M$	$\mu P$	$\mu S$	$L = l$	$L = 2l$	$L = 4l$
1	$x$	0	classical stretch	X	X	X	X	X	1.00	1.00	1.00
2	$y$	$x$	classical shear	X	X	X	X	X	1.00	1.00	1.00
3	$x^2$	0	inhomogeneous stretch reduced gradient $e_x$ -dir. microstretch	-	X	X	-	X	1.00	4.00	16.00
4	$y^2$	0	curvature (1)	-	X	C	C	-	1.00	4.00	16.00
5	$xy$	0	curvature (2) reduced gradient $e_y$ -dir. microstretch	-	X	X	C	X	1.00	4.00	16.00
6	$yz$	$xz$	twist	-	X	C	C	-	1.00	4.00	16.00
7	$yz$	$-xz$	torsion reduced gradient $e_z$ -dir. micropolar	-	X	X	X	-	1.00	4.00	16.00
8	$x^3$	0	microstretch (1)	-	-	X	-	X	1.00	16.00	256.00
	$\frac{3}{2}(xy^2 + xz^2)$	0	microstretch (2)	-	-	X	-	X	(1.48)	(23.68)	(378.93)
9	$y^3$	$x^3$	microshear (1)	-	-	X	-	-	(1.70)	(27.17)	(434.69)
	$x^2y$	$xy^2$	microshear (2)	-	-	X	-	-	1.00	16.00	256.00
	$3yz^2$	$3xz^2$	microshear (3)	-	-	X	-	-	(4.93)	(78.90)	(1262.45)
10	$y^3$	$-x^3$	micropolar (1)	-	-	X	X	-	1.00	16.00	256.00
	$x^2y$	$-xy^2$	micropolar (2)	-	-	X	X	-	(2.17)	(34.66)	(554.56)
	$3yz^2$	$-3xz^2$	micropolar (3)	-	-	X	X	-	(8.41)	(134.62)	(2153.97)
11	$xy^3$	$\frac{1}{4}x^4$	gradient $e_x$ -dir. microshear (1)	-	-	X	-	-	(2.89)	(23.13)	(11841.38)
	$\frac{1}{3}x^3y$	$\frac{1}{2}x^2y^2$	gradient $e_x$ -dir. microshear (2)	-	-	X	-	-	1.00	64.00	4096.00
	$3xyz^2$	$\frac{3}{2}x^2z^2$	gradient $e_x$ -dir. microshear (3)	-	-	X	-	-	(12.15)	(777.39)	(49753.28)
12	$y^3z$	$x^3z$	gradient $e_z$ -dir. microshear (1)	-	-	X	-	-	(1.62)	(103.98)	(6655.03)
	$x^2yz$	$xy^2z$	gradient $e_z$ -dir. microshear (2)	-	-	X	-	-	1.00	64.00	4096.00
	$yz^3$	$xz^3$	gradient $e_z$ -dir. microshear (3)	-	-	X	-	-	(1.32)	(84.71)	(5421.73)
13	$xy^3$	$-\frac{1}{4}x^4$	gradient $e_x$ -dir. micropolar (1)	-	-	X	X	-	{0.14}	{9.12}	{583.73}
	$\frac{1}{3}x^3y$	$-\frac{1}{2}x^2y^2$	gradient $e_x$ -dir. micropolar (2)	-	-	X	X	-	{(0.06)}	{(3.73)}	{(238.43)}
	$3xyz^2$	$-\frac{3}{2}x^2z^2$	gradient $e_x$ -dir. micropolar (3)	-	-	X	X	-	{(0.74)}	{(47.53)}	{(3042.20)}
14	$y^3z$	$-x^3z$	gradient $e_z$ -dir. micropolar (1)	-	-	X	X	-	{0.54}	{34.69}	{2220.14}
	$x^2yz$	$-xy^2z$	gradient $e_z$ -dir. micropolar (2)	-	-	X	X	-	{(0.61)}	{(39.29)}	{(2514.51)}
	$yz^3$	$-xz^3$	gradient $e_z$ -dir. micropolar (3)	-	-	X	X	-	{(0.84)}	{(53.93)}	{(3451.50)}
15	$xy$	$-\frac{1}{2}x^2$	reduced gradient $e_x$ -dir. micropolar	-	C	X	X	-	1.00	4.00	16.00

Table 7: homogeneous TVE

The last three columns of Table 7 show the energy per volume calculated for different sizes of TVEs, whereby  $L$  is the edge length of the cube used as TVE. The energy is normalised with respect to the smallest TVE ( $L = l$ ). The results show that for the linear modes the energy per volume remains constant for an increasing size of the TVE. This means that these deformation modes are not able to reflect size effects in the case of a homogeneous TVE as expected from the Boltzmann continuum theory. The quadratic deformation modes scale quadratically with the size of the TVE. This type of scaling is known from bending: if the diameter of a beam is scaled by a factor of two, the cross section is increased by a factor of 4 and the stiffness by a factor of 16. Calculating the energy per area, a factor of 4 remains. The cubic modes scale with the order  $2^4$ , and the quartic modes with the order  $2^6$ . So in general a mode of order  $n$  scales with the order  $2^{2(n-1)}$ .

As the results have shown, modes of the same order scale with exactly the same factor. Thus, it is always guaranteed that the deformation modes reflecting microstretch, microshear, and micropolar deformation for the smallest TVE are always the same for an arbitrary size of the TVE.

For the microstretch, microshear, and micropolar modes (no. 8 to 10) the results are normalised with respect to the respective weakest deformation mode of smallest size. This allows for a direct comparison of the deformation modes with respect to their stiffness. E. g., in the case of the microstretch the second mode is always about 1.48 times stiffer than the first mode. This factor is independent of the size of the TVE (differences occur due to truncation errors). While only one microstretch mode is needed by the macroscopic continuum theory, the weaker mode is chosen while the stiffer one is rejected. Rejection of a mode is indicated within the table by values set into round brackets "(•)". In the same way the results for microshear and micropolar deformations are presented. Thereby again the values of the rejected modes are set into round brackets.

Without competition the gradient of microstretch can be reflected by terms of second order instead of terms of fourth order (no. 3 and 5). Thus, the results for fourth order modes, which are able to reflect the gradient of microstretch deformation, are not presented. Due to the competition between the reduced gradient of second order for microshear and micropolar deformation modes, the complete results for the modes of fourth order are shown (no. 11 to 14). Thereby, the results of no. 11 and 13 as well as 12 and 14 (the gradient of the symmetric and the skew-symmetric part) are normalised with respect to the same value. So it can be directly seen that the gradient of the micropolar deformation always behaves more weakly than the gradient of the microshear deformation. Thus, the weaker deformation modes of fourth order (no. 13 and 14) are replaced by the corresponding modes of second order (no. 15 and 7). Indicating that the fourth order modes reflecting the gradient of micropolar deformation are not used, the values are set in curly brackets "{•}".

## 4.2 Plated TVE

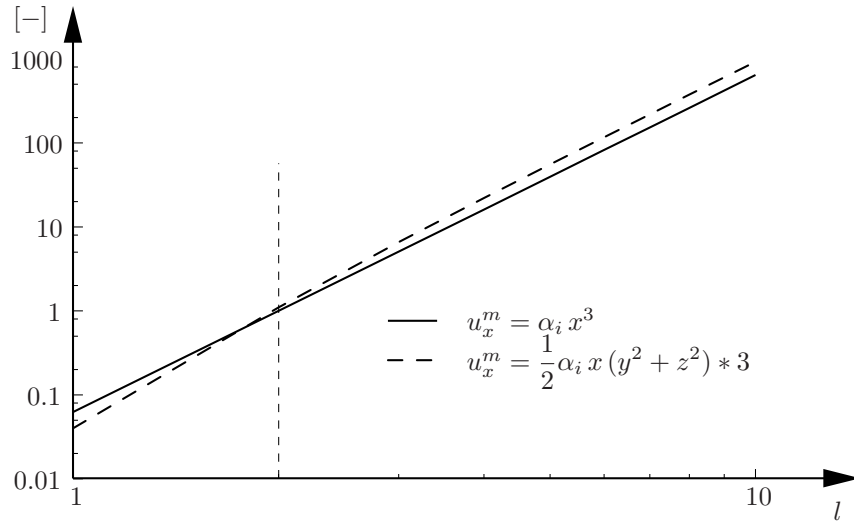
The second TVE under consideration is the plated TVE as shown in Figure 8.

While the TVE is not homogeneous, in a first step it is checked if the significant deformation mode for reflection of microstretch, microshear and micropolar deformation changes with the size of the TVE. Figure 9 shows the results for microstretch, microshear, and micropolar deformation varying the size of the TVE between  $L = l$  and  $L = 10l$  (value at  $L = 2l$  calibrated to 1). While in the case of microstretch deformation for the smallest TVE ( $L = l$ ) the mode presented in Figure 4 on the right is significant, for larger TVEs ( $L \geq 2l$ ) the mode in the same figure on the left behaves weaker and therefore it is chosen to reflect microstretch. The switch of the significant deformation mode is indicated by the dashed vertical line. The same effect can be observed for the microshear and micropolar deformation in Figure 9.

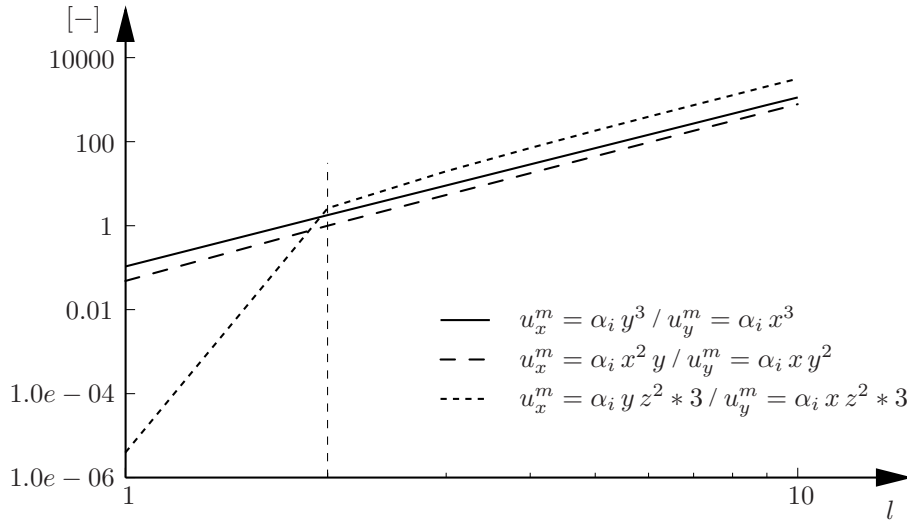
As already done before in the case of the homogeneous TVE, numerical tests are performed to calculate the energy associated with the certain deformation modes. However, for this example the energy is normalised with respect to the TVE of size  $L = 2l$  because the smallest TVE ( $L = l$ ) is acting an extra role: for some deformation modes the smallest TVE is significantly weaker than expected from the results from larger TVEs indicating a change of the load carrying behaviour. In these cases the smallest TVE carries the load by bending while for larger TVEs also stretching of the plates is involved. Furthermore the smallest TVE is not able to reflect the gradient of the second microshear and second micropolar deformation mode into  $e_x$ -direction because the displacement on the boundary of the TVE is zero. The changing load carrying behaviour can be seen quite well in Figure 9 for the microshear and for the micropolar deformation, but it appears also for other modes, e. g., no. 6 and 7 (twist and torsional deformation) presented in Table 8.

Due to the special role of the smallest TVE, it is now size dependent which is the significant mode for the reflection

Influence of TVE size for microstretch deformation



Influence of TVE size for microshear deformation



Influence of TVE size for micropolar deformation

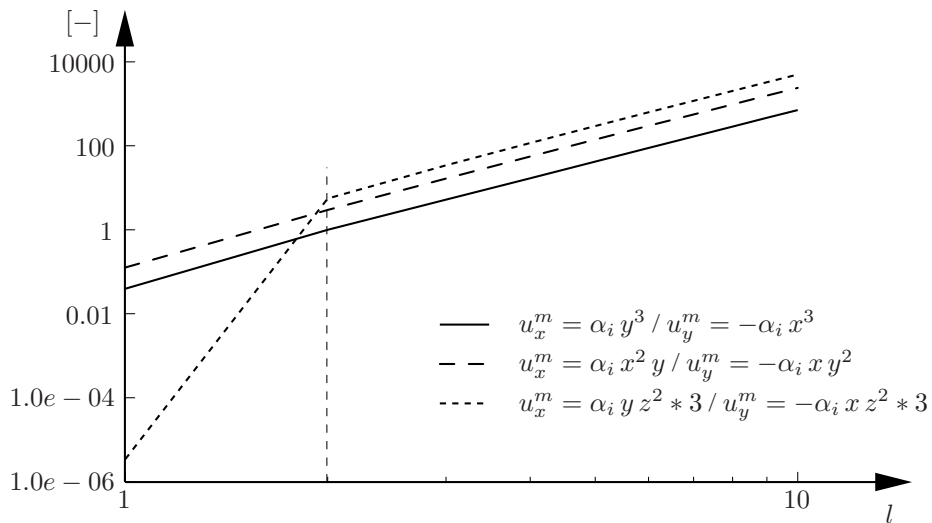


Figure 9: Influence of TVE size (plated microstructure)

no.	$u_x^m = \alpha_i \cdot \dots$	$u_y^m = \alpha_i \cdot \dots$	geometrical Interpretation	BCT	SGT	$\mu M$	$\mu P$	$\mu S$	$L = l$	$L = 2l$	$L = 4l$	$L = 8l$
1	$x$	0	classical stretch	X	X	X	X	X	1.00	1.00	1.00	1.00
2	$y$	$x$	classical shear	X	X	X	X	X	1.00	1.00	1.00	1.00
3	$x^2$	0	inhomogeneous stretch reduced gradient $e_x$ -dir. microstretch	-	X	X	-	X	0.248	1.0	4.300	18.524
4	$y^2$	0	curvature (1)	-	X	C	C	-	0.243	1.0	4.140	16.906
5	$xy$	0	curvature (2) reduced gradient $e_y$ -dir. microstretch	-	X	X	C	X	0.149	1.0	4.463	18.432
6	$yz$	$xz$	twist	-	X	C	C	-	4.445e-6	1.0	5.001	21.011
7	$yz$	$-xz$	torsion reduced gradient $e_z$ -dir. micropolar	-	X	X	X	-	5.352e-6	1.0	5.000	20.983
8	$x^3$	0	microstretch (1)	-	-	X	-	X	(0.063)	1.0	16.107	261.674
	$\frac{3}{2}(xy^2 + xz^2)$	0	microstretch (2)	-	-	X	-	X	0.040	(1.099)	(22.087)	(375.521)
9	$y^3$	$x^3$	microshear (1)	-	-	X	-	-	(0.107)	(1.782)	(28.710)	(463.387)
	$x^2y$	$xy^2$	microshear (2)	-	-	X	-	-	(0.048)	1.0	17.810	313.475
	$3yz^2$	$3xz^2$	microshear (3)	-	-	X	-	-	3.938e-6	(2.597)	(70.555)	(1278.448)
10	$y^3$	$-x^3$	micropolar (1)	-	-	X	X	-	(0.040)	1.0	16.894	286.583
	$x^2y$	$-xy^2$	micropolar (2)	-	-	X	X	-	(0.125)	(2.967)	(55.451)	(966.893)
	$3yz^2$	$-3xz^2$	micropolar (3)	-	-	X	X	-	3.414e-6	(5.541)	(116.200)	(2021.054)
11	$xy^3$	$\frac{1}{4}x^4$	gradient $e_x$ -dir. microshear (1)	-	-	X	-	-	(0.043)	(2.991)	(226.908)	(15800.057)
	$\frac{1}{3}x^3y$	$\frac{1}{2}x^2y^2$	gradient $e_x$ -dir. microshear (2)	-	-	X	-	-	(0.012)	1.0	74.918	5416.187
	$3xyz^2$	$\frac{3}{2}x^2z^2$	gradient $e_x$ -dir. microshear (3)	-	-	X	-	-	2.892e-7	(7.173)	(836.737)	(62690.413)
12	$y^3z$	$x^3z$	gradient $e_z$ -dir. microshear (1)	-	-	X	-	-	(2.468e-7)	(1.232)	(108.392)	(7668.498)
	$x^2yz$	$xy^2z$	gradient $e_z$ -dir. microshear (2)	-	-	X	-	-	(-)	1.0	81.281	5811.952
	$yz^3$	$xz^3$	gradient $e_z$ -dir. microshear (3)	-	-	X	-	-	3.572e-7	(0.774)	(80.688)	(6099.541)
13	$xy^3$	$-\frac{1}{4}x^4$	gradient $e_x$ -dir. micropolar (1)	-	-	X	X	-	{(0.023)}	{1.553}	{132.198}	{9578.835}
	$\frac{1}{3}x^3y$	$-\frac{1}{2}x^2y^2$	gradient $e_x$ -dir. micropolar (2)	-	-	X	X	-	{(0.010)}	{(0.900)}	{(70.620)}	{(5002.239)}
	$3xyz^2$	$-\frac{3}{2}x^2z^2$	gradient $e_x$ -dir. micropolar (3)	-	-	X	X	-	{2.892e-7}	{(6.233)}	{(636.539)}	{(45751.178)}
14	$y^3z$	$-x^3z$	gradient $e_z$ -dir. micropolar (1)	-	-	X	X	-	{(2.438e-7)}	{0.251}	{30.642}	{2482.035}
	$x^2yz$	$-xy^2z$	gradient $e_z$ -dir. micropolar (2)	-	-	X	X	-	{(-)}	{(0.955)}	{(77.675)}	{(5379.838)}
	$yz^3$	$-xz^3$	gradient $e_z$ -dir. micropolar (3)	-	-	X	X	-	{1.333e-7}	{(0.709)}	{(58.348)}	{(4051.920)}
15	$xy$	$-\frac{1}{2}x^2$	reduced gradient $e_x$ -dir. micropolar	-	C	X	X	-	0.140	1.0	4.455	18.299

Table 8: plated TVE

of microstretch, microshear and micropolar deformation (Table 8, no. 8, 9 and 10) also presented in Figure 9. The values corresponding to the significant modes are presented without brackets while the other modes are set into brackets. This setting of brackets is also applied to the gradient of the corresponding mode: if the micromode is not significant and therefore set into brackets, then also its gradients are set into brackets. This may lead to the result that the gradient of the micromode is not represented by the weakest deformation mode as can be seen for the gradient into  $e_z$ -direction of the microshear mode (no. 12). Another approach would be to decide independently which may be the significant gradient of microshear deformation again using the energy criterion.

As before in the case of the homogeneous TVE, the gradient modes of the micropolar deformation (Table 8, no. 13 and 14) are always weaker than the gradient modes of the microshear deformation (Table 8, no. 11 and 12) in the sense of consuming less energy. Thus, instead of the fourth order modes (no. 13 and 14) the according second order modes are used (no. 7 and 15).

Comparing the results for the plated TVE (Table 8) with the results for the homogeneous TVE (Table 7) one can observe that the values scale with about the same factor for increasing sizes of the TVE (excluding the smallest plated TVE). Thus, the principal deformation behaviour of the plated TVE is approximately the same as that one of the homogeneous TVE.

### 4.3 Cross-like TVE

The third TVE under consideration is a cross-like TVE as shown in Figure 8.

Again it is checked in a first step if the significant deformation mode for reflection of microstretch, microshear, and micropolar deformation changes with the size of the TVE. Figure 10 shows the results varying the size of the TVE between  $L = l$  and  $L = 10l$  (smallest value calibrated to 1). In the case of microstretch (upper part of Figure 10) for small TVEs ( $l \leq L \leq 3l$ ) the mode presented on the right hand side of Figure 4 is significant. For larger TVEs ( $L \geq 4l$ ) the mode in the same figure on the left hand side behaves weaker and therefore is chosen to reflect microstretch.

The same effect can be observed for microshear and micropolar deformations as shown in the middle of Figure 10 and the lower part of the same figure. In the case of microshear and micropolar deformation, three modes are, respectively, available to reflect the deformation, see Figure 5 and Figure 6.

Considering the effect that the deformation mode of interest depends on the size of the TVE, the according results for the cross-like microstructure are presented in Table 9. Applying the procedure with respect to the Boltzmann continuum theory on the macroscopic scale, moments on the boundary of the TVE cannot be handled by the homogenization procedure. Thus, in this case under consideration hinges at all beam ends on the boundary of the TVE, while in all other cases the rotational boundary conditions are calculated from the gradient of the displacement field (eq. (3)).

Again the gradient modes of the micropolar deformation (Table 9, no. 13 and 14) are weaker than the gradient modes of the microshear deformation (Table 9, no. 11 and 12) at least for the appropriate significant deformation mode. Thus, instead of the fourth order modes (no. 13 and 14), the according second order modes are used again (no. 7 and 15) as before for the homogeneous TVE and the plated TVE.

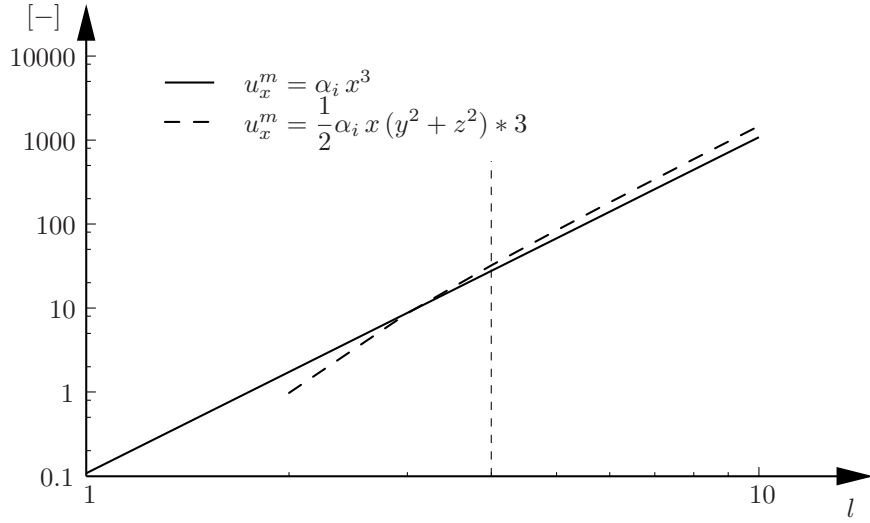
### 4.4 Star-like TVE (TVE with Negative Radical Strain Coefficient)

The last numerical example concerns the star-like TVE presented in Figure 8, whereby for a better understanding also the underlying 2-dimensional mechanism is presented. The main difference with respect to the previously discussed cross-like TVE, is the load carrying by bending instead of by stretching of the beam elements. Thus, the recent TVE behaves much more softly with respect to the stretching of the TVE. While the load is always carried by bending, it is not possible that the principal load carrying behaviour is changed when the size of the TVE is varied.

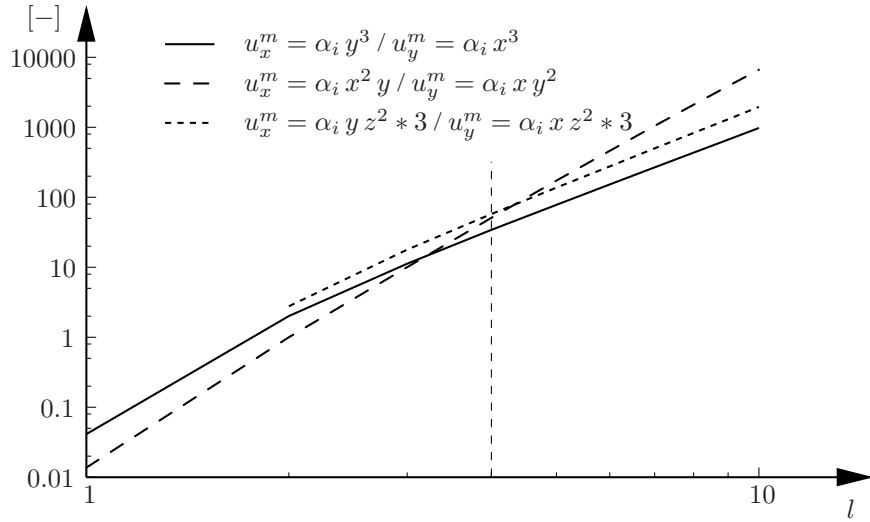
Again one observes that the significant mode representing microstretch, microshear, and micropolar deformation depends on the size of the TVE (Figure 11).

By taking a look on the gradient of the microshear and micropolar deformation (Table 10), one remarks that

Influence of TVE size for microstretch deformation



Influence of TVE size for microshear deformation



Influence of TVE size for micropolar deformation

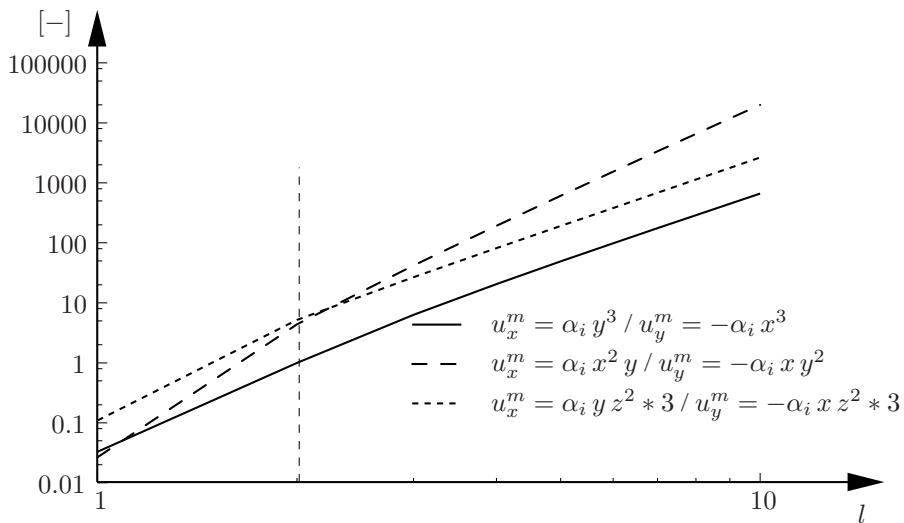
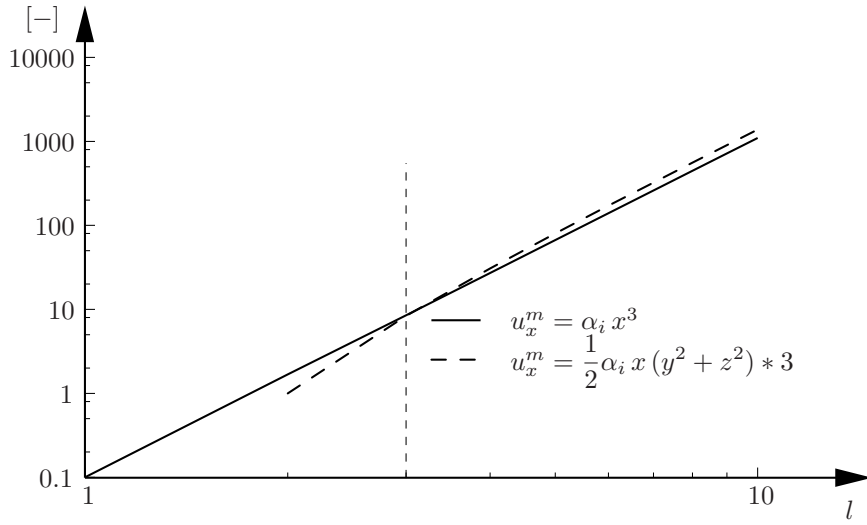


Figure 10: Influence of TVE size (cross-like microstructure)

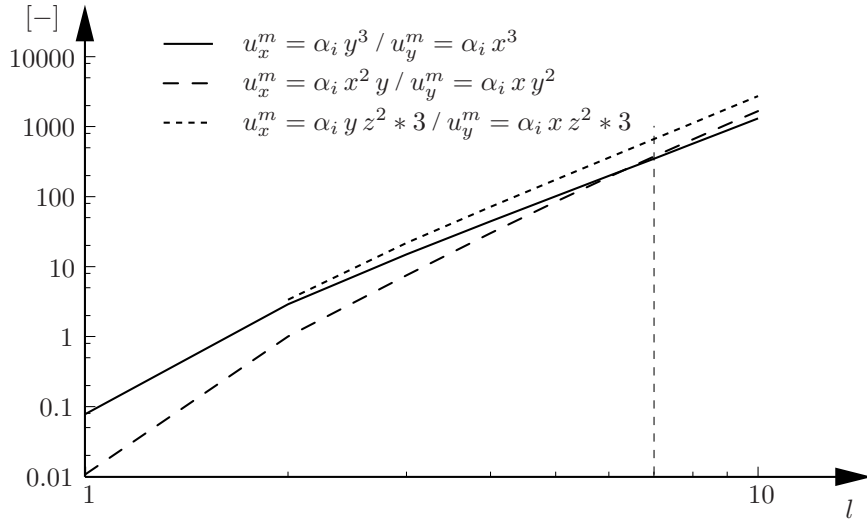
no.	$u_x^m = \alpha_i \cdot \dots$	$u_y^m = \alpha_i \cdot \dots$	geometrical Interpretation	BCT	SGT	$\mu M$	$\mu P$	$\mu S$	$L = l$	$L = 2l$	$L = 4l$	$L = 8l$
1 a	$x$	0	classical stretch	X	–	–	–	–	1.000	1.000	1.000	1.000
2 a	$y$	$x$	classical shear	X	–	–	–	–	1.000	1.000	1.000	1.000
1 b	$x$	0	classical stretch	–	X	X	X	X	1.00	1.000	1.000	1.000
2 b	$y$	$x$	classical shear	–	X	X	X	X	1.600	1.0	0.687	0.540
3	$x^2$	0	inhomogeneous stretch reduced gradient $e_x$ -dir. microstretch	–	X	X	–	X	0.304	1.0	7.751	60.512
4	$y^2$	0	curvature (1)	–	X	C	C	–	0.182	1.0	3.136	9.509
5	$xy$	0	curvature (2) reduced gradient $e_y$ -dir. microstretch	–	X	X	C	X	2.065e-4	1.0	4.998	20.987
6	$yz$	$xz$	twist	–	X	C	C	–	0.023	1.000	3.293	10.524
7	$yz$	$-xz$	torsion reduced gradient $e_z$ -dir. micropolar	–	X	X	X	–	0.235	1.000	3.658	13.033
8	$x^3$	0	microstretch (1)	–	–	X	–	X	(0.111)	(1.776)	28.420	455.205
	$\frac{3}{2}(xy^2 + xz^2)$	0	microstretch (2)	–	–	X	–	X	–	1.0	(32.966)	(608.202)
9	$y^3$	$x^3$	microshear (1)	–	–	X	–	–	(0.041)	(2.009)	34.064	433.975
	$x^2y$	$xy^2$	microshear (2)	–	–	X	–	–	0.014	1.0	(50.747)	(2105.386)
	$3yz^2$	$3xz^2$	microshear (3)	–	–	X	–	–	(–)	(2.778)	(57.394)	(832.700)
10	$y^3$	$-x^3$	micropolar (1)	–	–	X	X	–	(0.033)	1.0	20.499	288.931
	$x^2y$	$-xy^2$	micropolar (2)	–	–	X	X	–	0.027	(4.386)	(191.903)	(6559.345)
	$3yz^2$	$-3xz^2$	micropolar (3)	–	–	X	X	–	(0.109)	(18.907)	(281.529)	(3279.548)
11	$xy^3$	$\frac{1}{4}x^4$	gradient $e_x$ -dir. microshear (1)	–	–	X	–	–	(5.020e-5)	(1.0)	355.263	32472.107
	$\frac{1}{3}x^3y$	$\frac{1}{2}x^2y^2$	gradient $e_x$ -dir. microshear (2)	–	–	X	–	–	2.213e-5	1.717	(138.882)	(9590.917)
	$3xyz^2$	$\frac{3}{2}x^2z^2$	gradient $e_x$ -dir. microshear (3)	–	–	X	–	–	(–)	(8.741)	(1786.215)	(142013.310)
12	$y^3z$	$x^3z$	gradient $e_z$ -dir. microshear (1)	–	–	X	–	–	(0.003)	(2.671)	224.068	11999.897
	$x^2yz$	$xy^2z$	gradient $e_z$ -dir. microshear (2)	–	–	X	–	–	–	1.610	(460.303)	(83253.231)
	$yz^3$	$xz^3$	gradient $e_z$ -dir. microshear (3)	–	–	X	–	–	(–)	(1.0)	(102.561)	(6153.479)
13	$xy^3$	$-\frac{1}{4}x^4$	gradient $e_x$ -dir. micropolar (1)	–	–	X	X	–	{(5.020e-5)}	{0.977}	{352.900}	{32343.116}
	$\frac{1}{3}x^3y$	$-\frac{1}{2}x^2y^2$	gradient $e_x$ -dir. micropolar (2)	–	–	X	X	–	{2.213e-5}	{(1.723)}	{(139.882)}	{(9685.859)}
	$3xyz^2$	$-\frac{3}{2}x^2z^2$	gradient $e_x$ -dir. micropolar (3)	–	–	X	X	–	{(–)}	{(8.711)}	{(1781.450)}	{(141728.853)}
14	$y^3z$	$-x^3z$	gradient $e_z$ -dir. micropolar (1)	–	–	X	X	–	{(0.003)}	{0.686}	{67.075}	{4111.030}
	$x^2yz$	$-xy^2z$	gradient $e_z$ -dir. micropolar (2)	–	–	X	X	–	{(–)}	{(2.589)}	{(627.504)}	{(97133.229)}
	$yz^3$	$-xz^3$	gradient $e_z$ -dir. micropolar (3)	–	–	X	X	–	{(0.007)}	{(1.334)}	{(107.125)}	{(6127.210)}
15	$xy$	$-\frac{1}{2}x^2$	reduced gradient $e_x$ -dir. micropolar	–	C	X	X	–	2.083e-4	1.0	4.999	20.996

Table 9: cross-like TVE

Influence of TVE size for microstretch deformation



Influence of TVE size for microshear deformation



Influence of TVE size for micropolar deformation

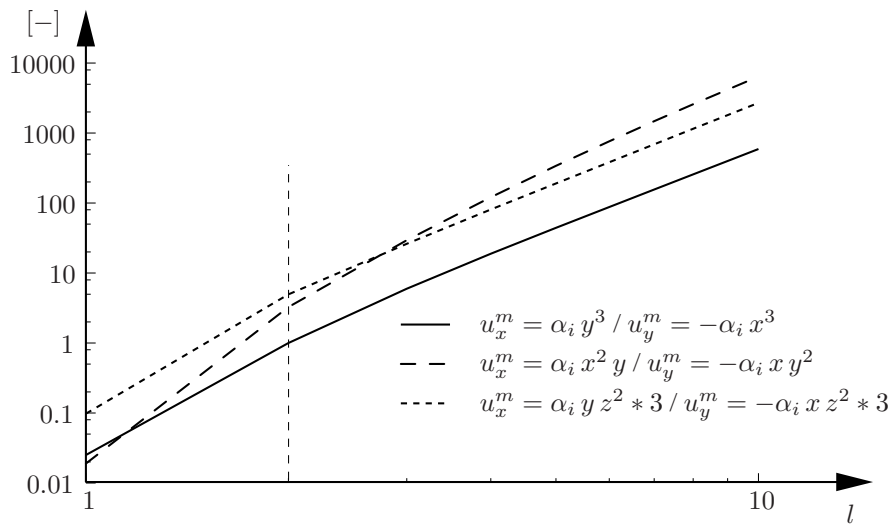


Figure 11: Influence of TVE size (star-like microstructure)

no.	$u_x^m = \alpha_i \cdot \dots$	$u_y^m = \alpha_i \cdot \dots$	geometrical Interpretation	BCT	SGT	$\mu M$	$\mu P$	$\mu S$	$L = l$	$L = 2l$	$L = 4l$	$L = 8l$
1 a	$x$	0	classical stretch	X	–	–	–	–	1.000	1.000	1.000	1.000
2 a	$y$	$x$	classical shear	X	–	–	–	–	1.000	1.000	1.000	1.000
1 b	$x$	0	classical stretch	–	X	X	X	X	1.00	1.000	1.000	1.000
2 b	$y$	$x$	classical shear	–	X	X	X	X	1.444	1.000	0.719	0.590
3	$x^2$	0	inhomogeneous stretch reduced gradient $e_x$ -dir. microstretch	–	X	X	–	X	0.312	1.000	6.026	28.316
4	$y^2$	0	curvature (1)	–	X	C	C	–	0.202	1.000	3.201	9.983
5	$xy$	0	curvature (2) reduced gradient $e_y$ -dir. microstretch	–	X	X	C	X	0.011	1.000	5.106	21.371
6	$yz$	$xz$	twist	–	X	C	C	–	0.019	1.000	3.454	11.781
7	$yz$	$-xz$	torsion reduced gradient $e_z$ -dir. micropolar	–	X	X	X	–	0.189	1.000	4.077	15.190
8	$x^3$	0	microstretch (1)	–	–	X	–	X	(0.100)	(1.678)	27.114	446.067
	$\frac{3}{2}(xy^2 + xz^2)$	0	microstretch (2)	–	–	X	–	X	–	1.000	(30.726)	(558.392)
9	$y^3$	$x^3$	microshear (1)	–	–	X	–	–	(0.078)	(2.893)	(44.273)	(570.962)
	$x^2y$	$xy^2$	microshear (2)	–	–	X	–	–	0.011	1.000	30.079	658.735
	$3yz^2$	$3xz^2$	microshear (3)	–	–	X	–	–	(–)	(3.370)	(71.265)	(1127.673)
10	$y^3$	$-x^3$	micropolar (1)	–	–	X	X	–	(0.025)	1.000	18.856	256.632
	$x^2y$	$-xy^2$	micropolar (2)	–	–	X	X	–	0.019	(3.263)	(121.187)	(2582.830)
	$3yz^2$	$-3xz^2$	micropolar (3)	–	–	X	X	–	(0.099)	(4.944)	(80.879)	(1147.874)
11	$xy^3$	$\frac{1}{4}x^4$	gradient $e_x$ -dir. microshear (1)	–	–	X	–	–	(0.002)	(2.434)	(382.437)	(28913.608)
	$\frac{1}{3}x^3y$	$\frac{1}{2}x^2y^2$	gradient $e_x$ -dir. microshear (2)	–	–	X	–	–	7.459e-4	1.000	98.256	7944.588
	$3xyz^2$	$\frac{3}{2}x^2z^2$	gradient $e_x$ -dir. microshear (3)	–	–	X	–	–	(–)	(8.342)	(1526.638)	(14184.297)
12	$y^3z$	$x^3z$	gradient $e_z$ -dir. microshear (1)	–	–	X	–	–	(0.003)	(3.126)	(238.419)	(13083.981)
	$x^2yz$	$xy^2z$	gradient $e_z$ -dir. microshear (2)	–	–	X	–	–	–	1.288	200.887	13744.223
	$yz^3$	$xz^3$	gradient $e_z$ -dir. microshear (3)	–	–	X	–	–	(–)	(1.0)	(89.225)	(5806.042)
13	$xy^3$	$-\frac{1}{4}x^4$	gradient $e_x$ -dir. micropolar (1)	–	–	X	X	–	{(0.002)}	{1.123}	{248.420}	{21220.670}
	$\frac{1}{3}x^3y$	$-\frac{1}{2}x^2y^2$	gradient $e_x$ -dir. micropolar (2)	–	–	X	X	–	{7.459e-4}	{(1.374)}	{(192.691)}	{(17028.628)}
	$3xyz^2$	$-\frac{3}{2}x^2z^2$	gradient $e_x$ -dir. micropolar (3)	–	–	X	X	–	{(–)}	{(5.801)}	{(1130.658)}	{(94613.614)}
14	$y^3z$	$-x^3z$	gradient $e_z$ -dir. micropolar (1)	–	–	X	X	–	{(0.004)}	{0.787}	{74.025}	{4593.780}
	$x^2yz$	$-xy^2z$	gradient $e_z$ -dir. micropolar (2)	–	–	X	X	–	{(–)}	{(2.249)}	{(444.169)}	{(19025.146)}
	$yz^3$	$-xz^3$	gradient $e_z$ -dir. micropolar (3)	–	–	X	X	–	{(0.007)}	{(1.609)}	{(124.464)}	{(7066.160)}
15	$xy$	$-\frac{1}{2}x^2$	reduced gradient $e_x$ -dir. micropolar	–	C	X	X	–	0.016	1.000	5.230	22.430

Table 10: star-like TVE

the gradient into  $e_x$ -direction of the microshear deformation (no. 11) is softer than that one of the micropolar deformation (no. 13) even for large sizes of the TVE. Thus, in contrast to the examples before, using the energy criterion, the gradient of the microshear deformation (no. 11) should be substituted by the according mode of second order. However, while for the component into  $e_z$ -direction it is exactly inverse, in analogy to the continuous TVE the gradient of the micropolar deformation is represented by terms of second order, while the gradient of the microshear deformation is reflected by terms of fourth order.

## 5 Conclusion

The numerical investigation of TVEs of different sizes gives information about the importance of the several deformation modes under consideration. This information can help to choose the continuum theory on a macroscopic level, which is able to reflect the recent effects.

Furthermore the considerations can be used to determine the required minimum size of a TVE reflecting the principal deformation behaviour. As shown in the examples, the smallest TVE under consideration does not reflect the principal deformation behaviour due to differences in the load carrying behaviour changing the size of the TVE.

The present kinematically based approach prescribing Dirichlet boundary conditions leads to an overestimation of the overall effective stiffness (Voigt bound). Thus, the approach can be improved using periodic boundary conditions.

## References

- Capriz, G.: *Continua with Microstructures*, vol. 35 of *Springer Tracts in Natural Philosophy*. Springer, New York (1980).
- Cosserat, E.; Cosserat, F.: *Théorie des corps déformables*. A. Hermann et Fils, Paris (1909).
- Eringen, C.: *Microcontinuum Field Theories, Vol. I: Foundations and Solids*. Springer-Verlag, Berlin (1999).
- Forest, S.: Aufbau und Identifikation von Stoffgleichungen für höhere Kontinua mittels Homogenisierungsstrategien. *Technische Mechanik*, 19, (1999), 297–306.
- Forest, S.; Barbe, F.; Cailletaud, G.: Cosserat modelling of size effects in the mechanical behaviour of polycrystals and multi-phase materials. *Int. J. Solids Structures*, 37, (2000), 7105–7126.
- Forest, S.; Sab, K.: Cosserat overall modeling of heterogeneous materials. *Mech. Res. Commun.*, 25, (1998), 449–454.
- Germain, P.: The method of displacement forces in the mechanics of continuous media: 1. second gradient theory. *J. Mecanique*, 12, (1973), 235–274.
- Huet, C.: An integrated micromechanics and statistical continuum thermodynamics approach for studying the fracture behaviour of microcracked heterogeneous materials with delayed response. *Eng. Fract. Mech.*, 58, (1997), 459–556.
- Nemat-Nasser, S.; Hori, M.: *Micromechanics*. North-Holland, Amsterdam (1993).

---

*Address:* T. Ebinger, Dr.-Ing. H. Steeb and Prof. Dr.-Ing. Stefan Diebels, Lehrstuhl für Technische Mechanik, Universität des Saarlandes, D-66041 Saarbrücken.

email: {t.ebinger; h.steeb; s.diebels}@mx.uni-saarland.de .